Article

Photoinduced Intramolecular Electron Transfer in Ruthenium and Osmium Polyads: Insights from Theory

Ilaria Ciofini, Philippe P. Lain, Fethi Bedioui, and Carlo Adamo

J. Am. Chem. Soc., **2004**, 126 (34), 10763-10777• DOI: 10.1021/ja0482278 • Publication Date (Web): 10 August 2004

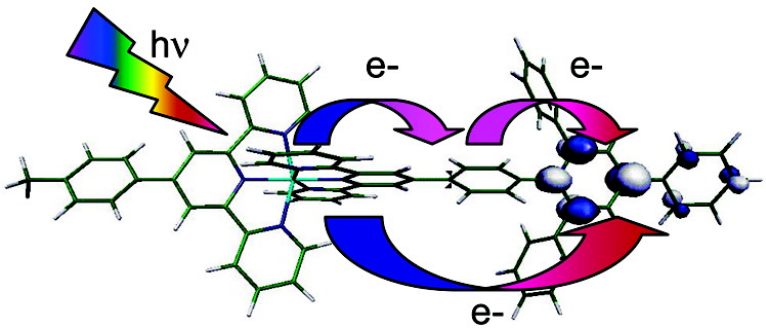

More About This Article

Additional resources and features associated with this article are available within the HTML version:

- Supporting Information
- Links to the 14 articles that cite this article, as of the time of this article download
- Access to high resolution figures
- Links to articles and content related to this article
- Copyright permission to reproduce figures and/or text from this article

View the Full Text HTML

J|A|C|S
ARTICLES
Published on Web 08/10/2004

Photoinduced Intramolecular Electron Transfer in Ruthenium and Osmium Polyads: Insights from Theory

Ilaria Ciofini,[†] Philippe P. Lainé,[‡] Fethi Bedioui,[§] and Carlo Adamo*[,†]

Contribution from the Laboratoire d'Électrochimie et Chimie Analytique, CNRS UMR-7575, École Nationale Supérieure de Chimie de Paris, 11 rue P. et M. Curie, F-75231, Paris Cedex 05, France; Laboratoire de Pharmacologie Chimique et Génétique CNRS FRE-2463 + INSERM U-640, École Nationale Supérieure de Chimie de Paris, 11 rue P. et M. Curie, F-75231, Paris Cedex 05, France; and Laboratoire de Chimie et Biochimie Pharmacologiques et Toxicologiques, CNRS UMR-8601, Université René Descartes, 45 rue des Saints Pères, F-75270, Paris Cedex 06, France

Received March 29, 2004; E-mail: adamo@ext.jussieu.fr

Abstract: Ru(II) and Os(II) complexes (P) of [4′-(*p*-phenyl)]terpyridyl ligand (ptpy) derivatized with an electron acceptor (A) of the triphenylpyridinium (H_3TP^+) type have been recently proposed as functional models for electron-transfer (ET) processes in the context of artificial photosynthesis. These inorganic dyads, P−A, are expected to undergo intramolecular photoinduced ET to form a charge separated (CS) state of pivotal interest. To draw a complete picture of possible ET processes, the ground- and excited-state properties of these complexes, both in their native and monoreduced forms, have been studied by the means of density functional theory (DFT). A time-dependent-DFT approach (TDDFT) was used to interpret the electronic spectra, while additional spectroscopic measurements have been carried out in order to complete the available experimental information and to further confirm the theoretical issues. Besides the noticeable quantitative agreement between computed and experimental absorption spectra, our results allow us to clarify, by first principles, the actual nature and interplay of the electronic and geometrical coupling between the acceptor moiety and the photosensitizer. The possibility of a direct (optical) ET from the ground state to the targeted *[P^+-A^-] CS state is theoretically postulated and found to be consistent with available photophysical data (transient absorption spectroscopy). Concerning backward ET (from the CS state), the occurrence of a quinoidal-like electronic redistribution inherent to the photoreduced acceptor-ligand is proposed to favor efficient charge recombination.

1. Introduction

The recent developments in the design, synthesis, and characterization of supramolecular architectures[1−4] allowed the construction of fairly sophisticated systems capable of selectively reacting to a given external input and behaving as devices at the molecular level.[5] In the case of photosensitized functional assemblies, so-called photochemical molecular devices (PMDs'),[4] the input is light and the response can be either a change in the structural features[6] or a change in the physicochemical properties.[7]

Among the basic light-triggered processes, the most widely studied ones are, by far, photoinduced electron transfers (PET) due to the prominent part they take in biological systems,[8] as well as in the intermingled research fields of molecular electronics[1−5,7,9−10] and photochemical conversion (and storage) of solar energy.[1,3,4,10−12] One of the major aims, when investigating functional model systems for artificial photosynthesis[13a] (as presently), is to build molecular assemblies showing photoinduced long-lived charge-separated (CS) states.[13b] Such excited states actually correspond to the transient conversion of light into an electrochemical potential, which can be used for energy storage[10,11,13,14] or electricity production.[12,15]

Specifically developed PMDs, generally referred to as *polyad* systems, are typically constituted by electron-donating (D) and/

[†] ENSCP/CNRS UMR-7575.
[‡] Université René Descartes.
[§] ENSCP/CNRS FRE-2463.

(1) (a) Lehn, J.-M. *Angew. Chem., Int. Ed. Engl.* **1990**, *29*, 1304−1319. (b) Lehn, J.-M. *Angew. Chem., Int. Ed. Engl.* **1988**, *27*, 89−112.
(2) Aviram, A.; Ratner, M. A. *Chem. Phys. Lett.* **1974**, *29*, 277−283.
(3) (a) Juris, A.; Balzani, V.; Barigelletti, F.; Belser, P.; Von Zelewsky, A. *Coord. Chem. Rev.* **1988**, *84*, 85−277. (b) Meyer, T. J. *Acc. Chem. Res.* **1989**, *22*, 163−170.
(4) (a) Balzani, V.; Juris, A.; Venturi, M.; Campagna, S.; Serroni, S. *Chem. Rev.* **1996**, *96*, 759−833. (b) Balzani, V.; Scandola, F. *Supramolecular Photochemistry*; Ellis Horwood: Chichester, U.K., 1991. (c) Balzani, V.; Moggi, L.; Scandola, F. In *Supramolecular Photochemistry*; Balzani, V., Ed; D. Reidel Publishing Co.: Dordrecht, The Netherlands, 1987; pp 1−28.
(5) De Silva, A. P.; McClenaghan, N. D. *Chem.—Eur. J.* **2004**, *10*, 574−586 and references therein. Kawai, T.; Iseda, T.; Irie, M. *Chem. Commun*. **2004**, 72−73. Ballardini, R.; Balzani, V.; Clemente-León, M.; Credi, A.; Gandolfi, M. T.; Ishow, E.; Perkins, J.; Stoddart, J. F.; Tseng, H.-R.; Wenger, S. *J. Am. Chem. Soc*. **2002**, *124*, 12786−12795 and references therein. Metzger, R. M. *Acc. Chem. Res*. **1999**, *32*, 950−957.
(6) For recent examples, see: (a) (conformation) Grabowski, Z. R.; Rotkiewicz, K.; Rettig, W. *Chem. Rev*. **2003**, *103*, 3899−4031. (b) (isomerization/folding) Cattani-Scholz, A.; Renner, C.; Cabrele, C.; Behrendt, R.; Oesterhelt, D.; Moroder, L. *Angew. Chem., Int. Ed*. **2002**, *41*, 289−292. (c) (isomerization/configuration) Rack, J. J.; Winkler, J. R.; Gray, H. B. *J. Am. Chem. Soc*. **2001**, *123*, 2432−2433. (d) (motion) Schofield, E. R.; Collin, J.-P.; Gruber, N.; Sauvage, J.-P. *Chem. Commun*. **2003**, 188−189. (e) (shuttling) Brouwer, A. M.; Frochot, C.; Gatti, F. G.; Leigh, D. A.; Mottier, L.; Paolucci, F.; Roffia, S.; Wurpel, G. W. H. *Science* **2001**, *291*, 2124−2128.

or -accepting (A) components together with a photosensitizing unit (P). Such systems can be defined, within the conceptual framework of supramolecular photochemistry,[4] as multicomponent systems, where the different units preserve their *functional* characteristics (namely their electronic properties) even when embedded in an assembly. The building blocks, preferably arranged in a linear fashion[11] according to the D−P−A sequence, are usually held together by covalent (but saturated) links, hydrogen bonding, or even mechanical contacts.[16] The overall working mechanism of a resulting prototypical triad, D−P−A, is also relatively well settled.[3,4,11,17] After light excitation of the P unit (the primary donor), a cascade of intramolecular electron transfers takes place, leading to the lower-lying CS state, $*[D^+-P-A^-]$. This state is then intended to be employed before charge recombination (CR) occurs.

A great deal of synthetic works have been carried out by experimentalists in the past decades to identify and select the different P, A, and D building blocks as well as to propose satisfactory intercomponent bridging units.[1,3,4,11,16−20] Although

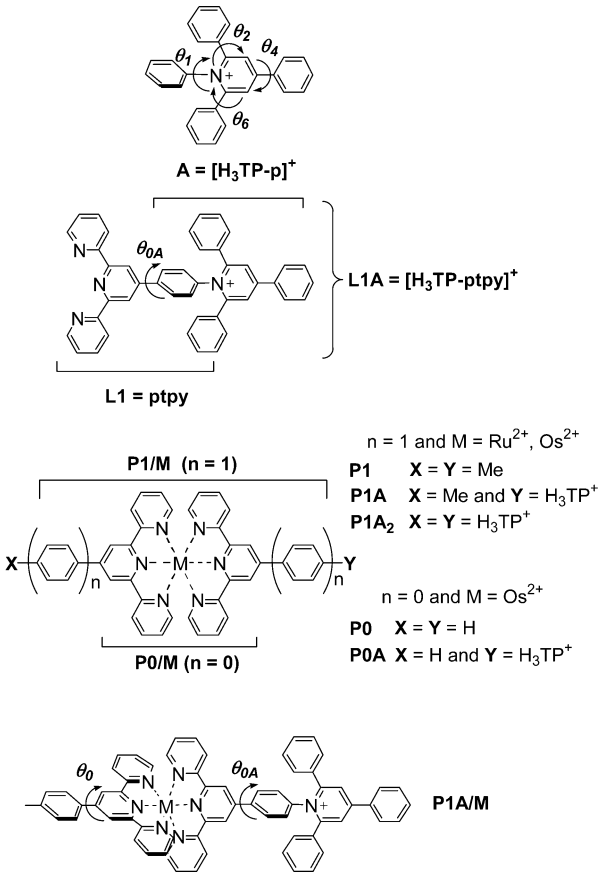

Figure 1. Schematic structures of organic and coordination compounds investigated along with their corresponding label and relevant angular parameters.

the nature of the various functional components is now well established, still a vivid activity[21] is going on to optimize them[22] and to adjust their relative "electronic" coupling.[23] Recently,[24] an electron-acceptor group (A) of the triphenylpyridinium type, $[H_3TP]^+$, was for the first time linked to the complex photosensitizer (P), $[M(tpy)_2]^{2+}$ (M = Ru(II), Os(II); tpy = 2,2′:6′,2″-terpyridine), both directly (**P0A/M**) and via a phenyl spacer (**P1A/M**, see Figure 1). These dyad systems are showing appealing structural[25] and photochemical properties.[26,27] They derive from a new family of triarylpyridinio-functionalized [4′-

(7) For recent examples, see: (a) (optical/photochromism) Irie, M. (Guest Editor) *Chem. Rev*. **2000**, *100*, 1683−1890. (b) (chiroptical) Feringa, B. L. *Acc. Chem. Res*. **2001**, *34*, 504−513. (c) (photochemical/luminescence) Wenger, O. S.; Henling, L. M.; Day, M. W.; Winkler, J. R.; Gray, H. B. *Inorg. Chem*. **2004**, *43*, 2043−2048. Miura, T.; Urano, Y.; Tanaka, K.; Nagano, T.; Ohkubo, K.; Fukuzumi, S. *J. Am. Chem. Soc*. **2003**, *125*, 8666−8671. Tyson, D. S.; Bignozzi, C. A.; Castellano, F. N. *J. Am. Chem. Soc*. **2002**, *124*, 4562−4563. (d) (NLO) Coe, B. J. *Chem.−Eur. J*. **1999**, *5*, 2464−2471. (e) (electrochemical) Mitchell, R. H.; Ward, R. T.; Chen, Y.; Wang, Y.; Weerawarna, S. A.; Dibble, P. W.; Marsella, M. J.; Almutairi, A.; Wang, Z.-Q. *J. Am. Chem. Soc*. **2003**, *125*, 2974−2988. (f) (electron transport) Andersson, M.; Sinks, L. E.; Hayes, R. T.; Zhao, Y.; Wasielewski, M. R. *Angew. Chem., Int. Ed*. **2003**, *42*, 3139−3143. Fraysse, S.; Coudret, C.; Launay, J.-P. *Eur. J. Inorg. Chem*. **2000**, 1581−1590. (g) (magnetism) Ratera, I.; Ruiz-Molina, D.; Vidal-Gancedo, J.; Novoa, J. J.; Wurst, K.; Létard, J.-F.; Rovira, C.; Veciana, J. *Chem.−Eur. J*. **2004**, *10*, 603−616. Sato, O. *Acc. Chem. Res*. **2003**, *36*, 692−700. Takayama, K.; Matsuda, K.; Irie, M. *Chem.−Eur. J*. **2003**, *9*, 5605−5609. Gütlich, P.; Garcia, Y.; Woike, T. *Coord. Chem. Rev*. **2001**, *219*, 839−879.

(8) Krauss, N. *Curr. Opin. Chem. Biol*. **2003**, *7*, 540−550. Willner, I.; Willner, B. *Coord. Chem. Rev*. **2003**, *245*, 139−151. Lubitz, W.; Lendzian, F.; Bittl, R. *Acc. Chem. Res*. **2002**, *35*, 313−320.

(9) (a) Joachim, C.; Gimzewski, J. K.; Aviram, A. *Nature* **2000**, *408*, 541−548. (b) Molecular Electronics. Launay, J.-P., Ed; *New J. Chem*. **1991**, *15* (special issue).

(10) (a) Gust, D.; Moore, T. A.; Moore, A. L. *Acc. Chem. Res*. **2001**, *34*, 40−48. (b) Barbara, P. F.; Meyer, T. J.; Ratner, M. A. *J. Phys. Chem*. **1996**, *100*, 13148−13168. (c) Hagfeldt, A.; Grätzel, M. *Chem. Rev*. **1995**, *95*, 49−68. (d) Bard, A. J.; Fox, M. A. *Acc. Chem. Res*. **1995**, *28*, 141−145. (e) Paddon-Row, M. N. *Acc. Chem. Res*. **1994**, *27*, 18−25. (f) Wasielewsky, M. R. *Chem. Rev*. **1992**, *92*, 435−461.

(11) (a) Baranoff, E.; Collin, J.-P.; Flamigni, L.; Sauvage, J.-P. *Chem. Soc. Rev*. **2004**, *33*, 147−155. (b) Collin, J.-P.; Gaviña, P.; Heitz, V.; Sauvage, J.-P. *Eur. J. Inorg. Chem*. **1998**, 1−14. (c) Sauvage, J.-P.; Collin, J.-P.; Chambron, J.-C.; Guillerez, S.; Coudret, C.; Balzani, V.; Barigelleti, F.; De Cola, L.; Flamigni, L. *Chem. Rev*. **1994**, *94*, 993−1019.

(12) (a) Imahori, H.; Norieda, H.; Yamada, H.; Nishimura, Y.; Yamazaki, I.; Sakata, Y.; Fukuzumi, S. *J. Am. Chem. Soc*. **2001**, *123*, 100−110. (b) Hagfeldt, A.; Grätzel, M. *Acc. Chem. Res*. **2000**, *33*, 269−277. (c) Bignozzi, C. A.; Argazzi, R.; Indelli, M. T.; Scandola, F. *Sol. Energy Mater. Sol. Cells* **1994**, *32*, 229−244. (d) O'Regan, B.; Grätzel, M. *Nature* **1991**, *353*, 737−740.

(13) (a) Sun, L.; Hammarström, L.; Åkermark, B.; Styring, S. *Coord. Chem. Rev*. **2001**, *30*, 36−49. (b) Hammarström, L. *Curr. Opin. Chem. Biol*. **2003**, *7*, 666−673.

(14) Chiorboli, C.; Fracasso, S.; Scandola, F.; Campagna, S.; Serroni, S.; Konduri, R.; MacDonnell, F. M. *Chem. Commun*. **2003**, 1658−1659.

(15) Hirata, N.; Lagref, J.-J.; Palomares, E. J.; Durrant, J. R.; Nazeeruddin, M. K.; Grätzel, M.; Di Censo, D. *Chem.−Eur. J*. **2004**, *10*, 595−602 and references therein. Loi, M. A.; Denk, P.; Hoppe, H.; Neugebauer, H.; Winder, C.; Meissner, D.; Brabec, C.; Sariciftci, N. S.; Gouloumis, A.; Vázquez, P.; Torres, T. *J. Mater. Chem*. **2003**, *13*, 700−704.

(16) Watanabe, N.; Kihara, N.; Furusho, Y.; Takata, T.; Araki, Y.; Ito, O. *Angew. Chem., Int. Ed*. **2003**, *42*, 681−683. Myles, A. J.; Branda, N. R. *J. Am. Chem. Soc*. **2001**, *123*, 177−178. Dürr, H.; Bossmann, S. *Acc. Chem. Res*. **2001**, *34*, 905−917 and references therein.

(17) Klumpp, T.; Linsenmann, M.; Larson, S. L.; Limoges, B. R.; Bürssner, D.; Krissinel, E. B.; Elliott, C. M.; Steiner, U. E. *J. Am. Chem. Soc*. **1999**, *121*, 1076−1087.

(18) Kurreck, H.; Huber, M. *Angew. Chem., Int. Ed*. **1995**, *34*, 849−866.

(19) Kalayanasundaram, K. *Photochemistry of Polypyridine and Porphyrin Complexes*, Academic Press: London, 1992.

(20) Imahori, H.; Sakata, Y. *Eur. J. Org. Chem*. **1999**, 2445−2457 and references therein.

(21) For instance, see: Borgström, B.; Johansson, O.; Lomoth, R.; Berglund Baudin, H.; Wallin, S.; Sun, L.; Åkermark, B.; Hammarström, L. *Inorg. Chem*. **2003**, *42*, 5173−5184.

(22) For examples, see: (a) (P unit) Polson, M.; Fracasso, S.; Bertolasi, V.; Ravaglia, M.; Scandola, F. *Inorg. Chem*. **2004**, *43*, 1950−1956. Passalacqua, R.; Loiseau, F.; Campagna, S.; Fang, Y.-Q.; Hanan, G. S. *Angew. Chem., Int. Ed*. **2003**, *42*, 1608−1611; Armaroli, N. *Chem. Soc. Rev*. **2001**, *30*, 113−124. (b) (D/A units) Siemeling, U.; Vor der Brüggen, J.; Vorfeld, U.; Neumann, B.; Stammler, A.; Stammler, H.-G.; Brockhinke, A.; Plessow, R.; Zanello, P.; Laschi, F.; Fabrizi de Biani, F.; Fontani, M.; Steenken, S.; Stapper, M.; Gurzadyan, G. *Chem.−Eur. J*. **2003**, *9*, 2819−2833. Li, K.; Schuster, D. I.; Guldi, D. M.; Herranz, M. A.; Echegoyen, L. *J. Am. Chem. Soc*. **2004**, *126*, 3388−3389.

(23) Selected examples: Rubtsov, I. V.; Redmore, N. P.; Hochstrasser, R. M.; Therien, M. J. *J. Am. Chem. Soc*. **2004**, *126*, 2684−2685. Weiss, E. A.; Chernick, E. T.; Wasielewski, M. R. *J. Am. Chem. Soc*. **2004**, *126*, 2326−2327. Claude, J. P.; Omberg, K. M.; Williams, D. S.; Meyer, T. J. *J. Phys. Chem. A* **2002**, *106*, 7795−7806. Holten, D.; Bocian, D. F.; Lindsey, J. S. *Acc. Chem. Res*. **2002**, *35*, 57−69. Guldi, D. M. *Coord. Chem. Rev*. **2002**, *31*, 22−36. Campagna, S.; Serroni, S.; Puntoriero, F.; Loiseau, F.; De Cola, L.; Kleverlaan, C. J.; Becher, J.; Sørensen, A. P.; Hascoat, P.; Thorup, N. *Chem.−Eur. J*. **2002**, *8*, 4461−4469. Kilså, K.; Kajanus, J.; Macpherson, A. N.; Mårtensson, J.; Albinsson, B. *J. Am. Chem. Soc*. **2001**, *123*, 3069−3080. Barigelletti, F.; Flamigni, L. *Chem. Soc. Rev*. **2000**, *29*, 1−12.

(24) Lainé, P.; Amouyal, E. *Chem. Commun*. **1999**, 935−936.

(*p*-phenyl)$_n$]terpyridyl ligands, $R^1{}_2R^2TP^+$-(p)$_n$tpy (here, $R^1 = R^2 =$ H and $n = 0, 1$), which has the valuable advantages, when complexed, of being structurally well-defined (rigid assembly) and, at the same time, of being chemically flexible (R^1, R^2). The synthetic versatility, which includes the metal cation (M) of P, allows the fine-tuning of the electronic and electrochemical properties of polyad systems. Also, the formation of redox cascades (P−A1−A2−...) is made possible for long-range and long-life CSs.[25,26] In fact, these triarylpyridinio-derivatized bisterpyridyl complexes of Ru(II) and Os(II) have been designed to satisfy two of the major criteria required for an efficient charge separation: (i) a rodlike shape and (ii) a controlled overall architecture. Both factors contribute to avoiding untimely withdrawal of the molecule that could favor charge recombination (intramolecular "short circuit").[28] Furthermore, the two bulky phenyl substituents ortho to the $N_{pyridinio}$ atom of the electron-acceptor group (A) prevent the pyridinium ring from adopting a coplanar conformation with the covalently linked photosensitizer unit (P1) and warrant the disruption of the conjugation between the two connected subunits. In other words, the necessary intercomponent *electronic decoupling* is expected to be produced by a *geometrical decoupling*,[29] which is playing the role usually fulfilled by saturated spacers. Experimentally, the effectiveness of such a correlation between structure and electronic properties has been demonstrated in the relaxed ground state for the acceptor dyads in their native form, **P1A/M**.[25,26] Nonetheless, the behavior of the electrochemically reduced forms, [**P1A/M**]$^-$, to some extent mimicking the targeted CS state, was remaining somewhat unclear.[26] The photophysical properties of the Os(II)-based dyad as well appeared a little disappointing even if thermodynamics for the charge-separation process was borderline (slightly endoergonic).[26]

At this stage, where experimental investigations are reaching their limits regarding their informative capability, a theoretical analysis of the problem to further gain new insights is mandatory. To correctly account for these phenomena, a theoretical method that is able to describe with comparable accuracy and, possibly, limited cost (due to the size of the system) both the ground and the excited states is needed.

Density functional theory (DFT) has been remarkably successful to accurately evaluate a variety of ground-state properties of large systems and, in particular, of complexes containing transition metals.[30−32] More recently, several papers have shown the potentialities of DFT, through the so-called time-dependent DFT approach (TD-DFT), for the study of excited states properties and, in particular, for the calculation of vertical electronic excitation spectra (see for instance refs 33−38). While DFT approaches have been successfully applied to the study of several Ru(II) and Os(II) polypyridyl complexes,[39−46] few applications were devoted to the analysis of excited states, the limiting factor being the size of the systems under investigation.[47−50] As a matter of fact, semiempirical approaches with all their own intrinsic limitations are still commonly used.[51,52] Unfortunately, the reliability of these methods is strictly bound to the quality of the parameters used, thus preventing routine applications.

This paper is aimed at using theoretical tools to gain insights into the physical chemistry and more specifically the electronic properties of the dyad systems (**P1A/M**) and related parent model compounds (**P1/M** and **A**; Figure 1). The ground-state properties of the various species both in their *native* and *reduced* forms (i.e. [**P1/M**]$^-$, [**A**]$^-$, and [**P1A/M**]$^-$), as well as their electronic absorption spectra, were particularly examined, to rationalize experimental results of a previous spectroelectrochemical study.[26] The behavior of the reduced systems is relevant in the studies of the spectroscopic properties of analogous CS excited states worth viewing as an intramolecular "light-induced" redox reaction (where A is reduced while P1 is oxidized).[53] From a qualitative viewpoint, our study allows us to establish, from first principles (i.e., ab initio), the nature of the coupling between the photosensitizer and the acceptor group within dyad systems and the role of the spacer (as bridging unit). It also feeds the discussion about the nature of the redox and photochemical processes taking place in the molecule. Thus, the theoretical information contributes to further substantiate or amend the interpretation of observed phenomena, only based

(25) Lainé, P.; Bedioui, F.; Ochsenbein, P.; Marvaud, V.; Bonin, M.; Amouyal, E. *J. Am. Chem. Soc.* **2002**, *124*, 1364−1377.
(26) Lainé, P.; Bedioui, F.; Amouyal, E.; Albin, V.; Berruyer-Penaud, F. *Chem.−Eur. J.* **2002**, *8*, 3162−3376.
(27) Konstantaki, M.; Koudoumas, E.; Couris, S.; Lainé, P.; Amouyal, E.; Leach, S. *J. Phys. Chem. B* **2001**, *105*, 10797−10804.
(28) Hu, Y.-Z.; Tsukiji, S.; Shinkai, S.; Oishi, S.; Hamachi, I. *J. Am. Chem. Soc.* **2000**, *122*, 241−253. Hu, Y.-Z.; Takashima, H.; Tsukiji, S.; Shinkai, S.; Nagamune, T.; Oishi, S.; Hamachi, I. *Chem.−Eur. J.* **2000**, *6*, 1907−1916.
(29) Johansson, O.; Borgström, M.; Lomoth, R.; Palmblad, M.; Bergquist, J.; Hammarström, L.; Sun, L.; Åkermark, B. *Inorg. Chem.* **2003**, *42*, 2908−2918.
(30) Koch, W.; Holthausen, M. C. *A Chemist's Guide to Density Functional Theory*; Wiley-VCH: Weinheim, Germany, 2000.
(31) Adamo, C.; di Matteo, A.; Barone, V. *Adv. Quantum Chem*. **1999**, *36*, 45−75.
(32) Burke, K.; Perdew, J. P.; Wang, Y. In *Electronic density functional theory: recent progress and new derivations*; Dobson, J. F., Vignale, G., Das, M. P., Eds.; Plenum Press: New York, 1997.
(33) (a) Boulet, P.; Chermette, H.; Daul, C. A.; Gilardoni, F.; Rogemond, F.; Weber, J.; Zuber, G. *J. Phys. Chem. A* **2001**, *105*, 885−894. (b) Boulet, P.; Chermette, H.; Weber, J. *Inorg. Chem.* **2001**, *40*, 7032−7039.
(34) Ciofini, I.; Adamo, C. *J. Chem. Phys. A* **2001**, *105*, 1086−1092.
(35) Cavillot, V.; Champagne, B. *Chem. Phys. Lett.* **2002**, *354*, 449−457.
(36) Adamo, A. Barone, V. *Theor. Chem. Acc.* **2000**, *105*, 169−172.
(37) Farrell, I. R.; van Slageren, J.; Zalis, S.; Vlcek, A. *Inorg. Chim. Acta* **2001**, *315*, 44−52.
(38) Jamorski Jödicke, C.; Lüthi, H. P. *J. Am. Chem. Soc.* **2003**, *125*, 252−264.
(39) Zheng, K.; Wang, J.; Shen, Y.; Peng, W.; Yun, F. *J. Comput. Chem*. **2002**, *23*, 436−443.
(40) Ziegler, M.; von Zelewsky, A. *Coord. Chem. Rev.* **1998**, *177*, 257−300.
(41) Broo, A.; Lincoln, P. *Inorg. Chem.* **1997**, *36*, 2544−2553.
(42) Damrauer, N. H.; Boussie, T. R.; Deveney, M.; McCusker, J. K. *J. Am. Chem. Soc.* **1997**, *119*, 8253−8268.
(43) Wakatsuki, Y.; Koga, N.; Yamazaki, H.; Morokuma, K. *J. Am. Chem. Soc.* **1994**, *116*, 8105−8111.
(44) Zhang, L. T.; Ko, J.; Ondrechen, M. J. *J. Am. Chem. Soc.* **1987**, *109*, 1666−1671.
(45) (a) Daul, C.; Baerends, E. J.; Vornooijs, P. *Inorg. Chem.* **1994**, *33*, 3538−3543. (b) Albano, G.; Belser, P.; Daul, C. A. *Inorg. Chem*. **2001**, *40*, 1408−1413. (c) Fantacci, S.; De Angelis, F.; Selloni, A. *J. Am. Chem. Soc.* **2003**, *125*, 4381−4387.
(46) Seneviratne, D. S.; Uddin, Md. J.; Swayambunathan, V.; Schlegel, H. B.; Endicott, J. F. *Inorg. Chem*. **2002**, *41*, 1502−1517.
(47) Hay, P. J. *J. Phys. Chem. A* **2002**, *106*, 1634−1641.
(48) Guillemoles, J.-F.; Barone, V.; Joubert, L.; Adamo, C. *J. Phys. Chem. A* **2002**, *106*, 11354−11360.
(49) Monat, J.; Rodriguez, J. H.; McCusker, J. K. *J. Phys. Chem. A* **2002**, *106*, 7399−7406.
(50) (a) Hazebroucq, S.; Joubert, L.; Ciofini, I.; Adamo, C. *Theor. Chem. Acc.* **2004**, in press. (b) Ciofini, I.; Daul, C.; Adamo, C. *J. Phys. Chem. A* **2003**, *107*, 11182−11190.
(51) (a) Nazeeruddin, Md. K.; Zakeeruddin, S. M.; Humphry-Baker, R.; Gorelsky, S. I.; Lever, A. B. P.; Grätzel, M. *Coord. Chem. Rev.* **2000**, *208*, 213−225. (b) Fiebig, T.; Wan, C.; Kelly, O. S.; Barton, J. K.; Zewail, A. H. *Proc. Natl. Acad. Sci. U.S.A.* **1999**, *96*, 1187−1192.
(52) (a) Estiú, G.; Cukiernik, F. D.; Maldivi, P.; Poizat, O. *Inorg. Chem.* **1999**, *38*, 3030−3039. (b) Amini, A.; Harriman, A. *J. Phys. Chem. A* **2004**, *108*, 1242−1249.
(53) McCusker, J. *Acc. Chem. Res*. **2003**, *36*, 876−887.

on experimental issues,[26] and provides a deeper understanding of the nature of the excited states.

2. Computational Methods

All calculations were carried out using a development version of the Gaussian code.[54] A recent hybrid Hartree−Fock/density functional model, referred to as PBE0, was used.[55] This approach was obtained by casting the PBE exchange and correlation functional[56] in a hybrid DFT/HF scheme, where the HF/DFT exchange ratio is fixed a priori to 1:4.[57]

In the case of open shell systems, unrestricted calculations were performed and spin contamination, monitored by the expectation value of S^2, was found to be negligible.

A double ζ quality LANL2 basis,[58] and corresponding pseudopotentials for the metal atoms (Os and Ru),[59] was used for all atoms for both the structural optimizations and the calculation of the electronic properties. Such a level of theory (DFT + LANL2DZ basis set) has previously been successfully applied in a few works concerning the structure, spectroscopic properties, and reactivity of organometallic systems.[33,50]

The molecular structure of each organic molecule and coordination compound was fully optimized; C_2 symmetry constraints were imposed for **P1/M** systems (M = Ru, Os), while all other systems were computed without symmetry constraints. Only in the case of reduced **P1A/Os**, the optimized structure of the corresponding native form was used when computing the electronic absorption spectrum.

Optical transitions were computed using the time-dependent DFT approach as implemented in the Gaussian program.[60] From these calculations, two quantities, related to the UV−vis spectra, are readily available: the energy of any electronic $E^{00}_{n\rightarrow m}$ transition and the corresponding oscillator strength (*f*). Based on these quantities, the spectra were afterward simulated, using Gaussian functions, to have a direct comparison with the experimental data. Since the integral of these Gaussian functions is proportional to the oscillator strength of associated electronic transitions,[61] the only adjustable parameter is the full width at half-maximum (fwhm), that is, the broadening of each peak (individual transition). This broadening is mainly related to both the populations of the vibronic/rotation levels and the solvent effects. It is also strongly varying from a transition to another and a fortiori from a system to another.[46] At the same time, *experimental* absorption bands, like MLCTs, generally result from the sum of many and various transitions, thus making the fwhm parameters not directly attainable from experimental data. To circumvent these problems, a fixed bandwidth is usually assumed for this kind of complexes, of about 0.4 eV.[53,62] We, instead, used different fwhm's for the different systems, and a satisfactory matching of the computed spectrum with the experimental trace was found with smaller fwhm parameters, ranging between 0.1 and 0.2 eV.

The accuracy of the theoretical method concerning the energy of the various electronic transitions was reflected not only by the overall shape of the resulting simulated absorption bands but also by the energy at their maximum ($E^{\max}_{\mathrm{calcd}}$) as compared to the corresponding experimental band maxima ($E^{\max}_{\mathrm{expt}}$). This mismatch was quantified via a reliability factor, *R* (%), as follows:

$$R = \frac{E^{\max}_{\mathrm{calcd}} - E^{\max}_{\mathrm{expt}}}{E^{\max}_{\mathrm{expt}}} \times 100$$

In the present study, the calculations were restricted to electronic transitions of energy lower than 4.1 eV (about 300 nm) for all organic molecules and below 3.1 eV (about 400 nm) for the inorganic compounds.[63] Among all of the electronic transitions calculated, only the principal ones were reported in the tables. Noteworthy, the fact that the present theoretical method does not take into account solvent effects is not detrimental to the relevance of calculated issues, as complexes studied exhibit almost no solvatochromism, at least in their native form, in contrast with other ruthenium complexes.[48]

3. Experimental Procedure

In situ spectroelectrochemical measurements were carried out in a homemade cell constituted from a standard UV−visible cuvette (pathway length of 1 cm and total solution volume of 5.5 mL) which was opened out on its top to make easy the introduction of the working, reference, and counter electrodes.[26] The working electrode was a platinum grid of a geometrical area of 3 cm^2, which was flattened against one of the walls of the cuvette opposite to the light beam pathway. A platinum wire was used as the counter electrode, and a homemade AgCl-coated Ag wire, as the reference electrode. The potential difference between this reference electrode and SCE was equal to 30 mV, and it was checked daily, before and after use. Electrolytic solutions were routinely deoxygenated with argon and kept under inert atmosphere during the experiments. UV−visible absorption spectra were recorded by using a Shimadzu UV-160A spectrophotometer. Data were collected between 200 and 900 nm for the compounds in their native form but only between 350 and 900 nm for their corresponding reduced forms, due to the experimental setup of spectroelectrochemistry.

Transient absorption spectra were recorded as described in ref 26.

4. Results

As mentioned above, we have studied the characteristic physical and chemical properties of several reference organic and inorganic molecules, including a more complex two-component (so-called *dyad*) supramolecular system built up from the association of the previous parent photosensitizer and acceptor units. The various species under investigation are depicted in Figure 1, along with abbreviations used.

Efficient PMDs specifically designed for artificial photosynthesis purposes are characterized by fast intramolecular PET processes and long-life CS states. Of importance, electronic interactions between the different subunits must be very weak, so as to favor a stepwise localization of the hopping electron and retard charge recombination.[11] Such a critical intercomponent *decoupling* has been evaluated at three different, and interrelated, levels: structural (section 4.1), electronic (section 4.2), and spectroscopic (sections 4.3−4.5).

(54) Frisch, M. J.; Trucks, G. W.; Schlegel, H. B.; Scuseria, G. E.; Robb, M. A.; Cheeseman, J. R.; Montgomery, J. A., Jr.; Vreven, T.; Kudin, K. N.; Burant, J. C.; Millam, J. M.; Iyengar, S. S.; Tomasi, J.; Barone, V.; Mennucci, B.; Cossi, M.; Scalmani, G.; Rega, N.; Petersson, G. A.; Nakatsuji, H.; Hada, M.; Ehara, M.; Toyota, K.; Fukuda, R.; Hasegawa, J.; Ishida, M.; Nakajima, T.; Honda, Y.; Kitao, O.; Nakai, H.; Li, X.; Knox, J. E.; Hratchian, H. P.; Cross, J. B.; Adamo, C.; Jaramillo, J.; Gomperts, R.; Stratmann, R. E.; Cammi, R.; Pomelli, C.; Ochterski, J.; Ayala, P. Y.; Morokuma, K.; Hase, W. L.; Salvador, P.; Dannenberg, J. J.; Zakrzewski, V. G.; Dapprich, S.; Daniels, A. D.; Strain, M. C.; Farkas, O.; Malick, D. K.; Rabuck, A. D.; Raghavachari, K.; Foresman, J. B.; Ortiz, J. V.; Cui, Q.; Baboul, A. G.; Clifford, S.; Cioslowski, J.; Stefanov, B. B.; Liu, G.; Liashenko, A.; Piskorz, P.; Komaromi, I.; Martin, R. L.; Fox, D. J.; Keith, T.; Al-Laham, M. A. C.; Peng, Y.; Nanayakkara, A.; Challacombe, M.; Gill, P. M. W.; Johnson, B.; Chen, W.; Wong, M. W.; Gonzalez, C.; Pople, J. A. *Gaussian Development Version*, revision A.01; Gaussian, Inc.: Pittsburgh, PA, 2003.
(55) Adamo, C.; Barone, V. *J. Chem. Phys.* **1999**, *110*, 6158−6170.
(56) Perdew, J. P.; Burke, K.; Ernzerhof, M. *Phys. Rev. Lett.* **1996**, *77*, 3865−3868.
(57) Adamo, C.; Barone, V. *Chem. Phys. Lett.* **1997**, *274*, 242−250.
(58) Dunning, T. H., Jr.; Hay, P. J. In *Modern Theoretical Chemistry*; Schaefer, H. F., III, Ed.; Plenum: New York, 1976; pp 1−28.
(59) Hay, J.; Wadt, W. R. J. *Chem. Phys.* **1985**, *82*, 299−310.
(60) Stratmann, R. E.; Scuseria, G. E.; Frisch, M. *J. Chem. Phys.* **1998**, *109*, 8128−8224.
(61) Sandorfly, C. *Electronic Spectra and Quantum Chemistry*; Prentice-Hall: Englewood Cliffs, New Jersey, 1964.
(62) Gorelsky, S. I.; Lever, A. B. P.; Ebadi, M. *Coord. Chem. Rev.* **2002**, *230*, 97−105.
(63) For **P1A/Os**, transitions were calculated up to ca. 3.5 eV, i.e., 350 nm.

Table 1. Main Computed Structural Parameters (Distances in Å, Angles in degrees)[h]

	A[a]	**[A]$^-$**	**L1A**[b]	**[L1A]$^-$**
$d(N_{py+}-C_{Ar})$	1.470 (1.460)	1.4350	1.461 (1.440)	1.4307
θ_1	69.6 (77.5)	57.4	66.9 (72.6)	54.3
θ_2	60.0 (71.75)[c]	50.6	56.9 (63.7)[c]	53.2
θ_6	61.0 (71.75)[c]	50.6	53.0 (63.7)[c]	52.2
θ_4	29.4 (22.5)	15.8	28.3 (16.5)	14.7

	P1/Ru[d]	**[P1/Ru]$^-$**	**P1/Os**[e]	**[P1/Os]$^-$**
$d(M-N_2)$	2.082 (2.067)	2.073	2.066 (2.059)	2.056
$d(M-N_1)$	1.990 (1.985)	1.984	1.988 (1.972)	1.981
$\alpha(N_1-M-N_2)$	78.9 (79.7)	79.0	78.7 (78.9)	78.9
θ_0	30.5 (35.8)	32.5	30.6 (- -)	32.7

P1A/Os[f]

$d(N_{py+}-C_{Ar})$	1.4584 (- -)	θ_{0-P1}	29.3 (- -)
$d(M-N_2)$	2.069 (- -)	θ_{0-P1A}	35.9 (35.6)
$d(M-N_1)$	1.999 (1.963)	θ_1	67.3 (86.7)
$d(M-N_{2(A)})$[g]	2.063 (2.036)	θ_2	60.9 (73.4)[c]
$d(M-N_{1(A)})$[g]	1.979 (1.963)	θ_6	56.3 (73.4)[c]
		θ_4	24.46 (24.5)

[a] From refs 64 and 65. [b] From ref 25. [c] $(\theta_2 + \theta_6)/2$. [d] X-ray data of **P1-R/Ru** (R is an aza-crown macrocyclic fragment) from ref 66. [e] X-ray data of **P0/Os** from ref 67. [f] X-ray data of **P1A$_2$/Ru** from ref 25. [g] $N_{1(A)}$ and $N_{2(A)}$ refer to N_{tpy} atoms of L1A ligand. [h] The experimental X-ray data of the compounds or related systems are reported in parenthesis. For nomenclature, refer to Figure 1 and text (section 4.1).

4.1. Structural Features: Geometrical Decoupling. Computed structural features of the 1,2,4,6-tetraphenylpyridinium isolated model acceptor ($[H_3TP\text{-}p]^+$ = **A**) and related ligand ($[H_3TP\text{-}ptpy]^+$ = **L1A**) together with those of the **P1/M** complexes (both in their ground-state *native* and *reduced* forms) and acceptor-dyad **P1A/Os** are reported in Table 1. Available experimental data concerning the structure of the molecules examined or other close structural analogues are also gathered in Table 1 for comparison purposes.

In the case of the organic species **A** and **L1A** in their native form, there is a rather good agreement between computed and X-ray structures.[25] For instance, the length of the bond that connects the $N_{pyridinio}$ atom of the acceptor to the phenyl spacer of L1 within **L1A**, $C_{py+}-N_{Ar}$, is reproduced within 0.02 Å of accuracy. Regarding the various dihedral angles defined between the plane of the central pyridinium ring and the planes of its phenyl substituents (θ_1, θ_2, θ_4, and θ_6), slight negative deviations can be noticed in most cases, the largest difference being computed for θ_4 (11.9°). Although these small deviations are within the range of accuracy expected in the structural prediction of floppy motions at the level of theory used, it is worth noting that θ_4 is also typically one of those molecular parameters that is more affected by packing forces in crystal structures.[68a]

Upon single-electron reduction, [**A**]$^-$ and [**L1A**]$^-$ are found to become significantly more flattened. In particular, the twist angle θ_1 between the phenyl (spacer) and the pyridinium ring decreases by about 12.5°. At the same time, a significant shortening of the $C_{py+}-N_{Ar}$ bond (0.02 and 0.08 Å, respectively) is found. A detailed analysis of the bond length pattern calculated for the two reduced species also reveals alternate short and long bond lengths for the pyridinium ring (and spreading toward the tpy fragment for [**L1A**]$^-$; see Supporting Information), consistent with a quinoidal contribution.[69] The most relevant postulated limiting canonical forms of [**L1A**]$^-$ are represented in Scheme 1.

Scheme 1

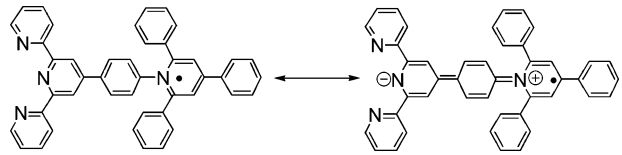

Concerning the metal complexes, the computed structural parameters were compared to those of close structural analogues, since the X-ray structures of the isolated parent species are not available. In **P1/M**, the direct environment of the metal cation exhibits a pseudo-octahedral (D_{2d}) symmetry, with shorter $M-N_{tpy}$ bonds along the main axis (that is the one passing by the metal and the nitrogen atoms, N1, of the central pyridine ring of each tpy), in agreement with previous experimental findings.[25] For instance, in the case of **P1/Ru**, the shorter (Ru−N1) and longer (Ru−N2) types of bonds (Figure 1) are found to be 1.990 Å and 2.082 Å, respectively, close to the average values measured for similar systems (1.977 Å and 2.068 Å, respectively).[25,68b] As previously noticed for the free ligand, the calculated dihedral angle between the tpy plane and the phenyl ring of the ptpy ligand within P1 (θ_0; Figure 1) is found to slightly deviate (about 5°) from that determined in the solid-state X-ray structure ($\theta_0 = 24.81°$; average value).[25] However, it remains in the expected range compatible with the well-established π-extending role of the phenyl that allows an electronic delocalization over the entire ptpy system.[25,70]

No significant variation in the coordination sphere of Ru(II) can be found upon the monoelectronic reduction of P1, the maximum variation of $M-N_{tpy}$ bond lengths being 0.02 Å. This fact is not surprising for a process essentially located on the rigid (p)tpy ligands. It is worth noting that, in the striking case of the two-times reduced $[Ru(bpy)_3]^0$ complex (a possible electride species), electrochemically generated and structurally characterized by X-ray analysis,[71] such an almost negligible structural reorganization was also evidenced.

Similar trends are found for the **P1/Os** analogue, characterized by a pseudo-octahedral metal coordination and Os−N bond lengths very close to those experimentally observed for **P0/Os** (see Table 1).[67] The computed structural relaxation induced by the reduction was also found to be negligible, as is the case for [**P1/Ru**]$^-$.

Upon derivatization of ligand L1 by the H_3TP^+ moiety (dyad **P1A/Os**), no significant change in the direct coordination sphere of the Os(II) cation was computed. Nevertheless, when going from **P1/Os** to **P1A/Os**, the dihedral angle defined by each tpy plane and its attached phenyl ring (spacer) within the P1 unit (θ_0, Figure 1, Table 1) was found to be larger for the phenyl

(64) Farag, I. S. A.; El-Shora, A. I.; Rybakov, V. B. *Cryst. Res. Technol.* **1990**, *25*, 519−524.
(65) Othman, A. H.; Zakaria, Z.; Ng, S. W. *J. Crystallogr. Spectrosc. Res.* **1993**, *23*, 921.
(66) Bushell, K. L.; Couchman, S. M.; Jeffery, J. C.; Rees, L. H.; Ward, M. D. *J. Chem. Soc., Dalton Trans.* **1998**, 3397−3403.
(67) Craig, D. C.; Scudder, M. L.; McHale, W. A.; Goodwin, H. A. *Aust. J. Chem.* **1998**, *51*, 1131−1139.
(68) (a) Adamo, C.; di Matteo, A.; Rey, P.; Barone, V. *J. Phys. Chem. A* **1999**, *103*, 3481−3488. (b) Alcock, N. W.; Barker, P. R.; Haider, J. M.; Hannon, M. J.; Painting, C. L.; Pikramenou, Z.; Plummer, E. A.; Rissanen, K.; Saarenketo, P. *J. Chem. Soc., Dalton Trans.* **2000**, 1447−1461.
(69) Karafiloglou, P. *Chem. Phys.* **1997**, *214*, 171−182.
(70) Collin, J.-P.; Guillerez, S.; Sauvage, J.-P.; Barigelletti, F.; De Cola, L.; Flamigni, L.; Balzani, V. *Inorg. Chem.* **1991**, *30*, 4230−4238.
(71) Pérez-Cordero, E. E.; Campana, C.; Echegoyen, L. *Angew. Chem., Int. Ed.* **1997**, *36*, 137−140.

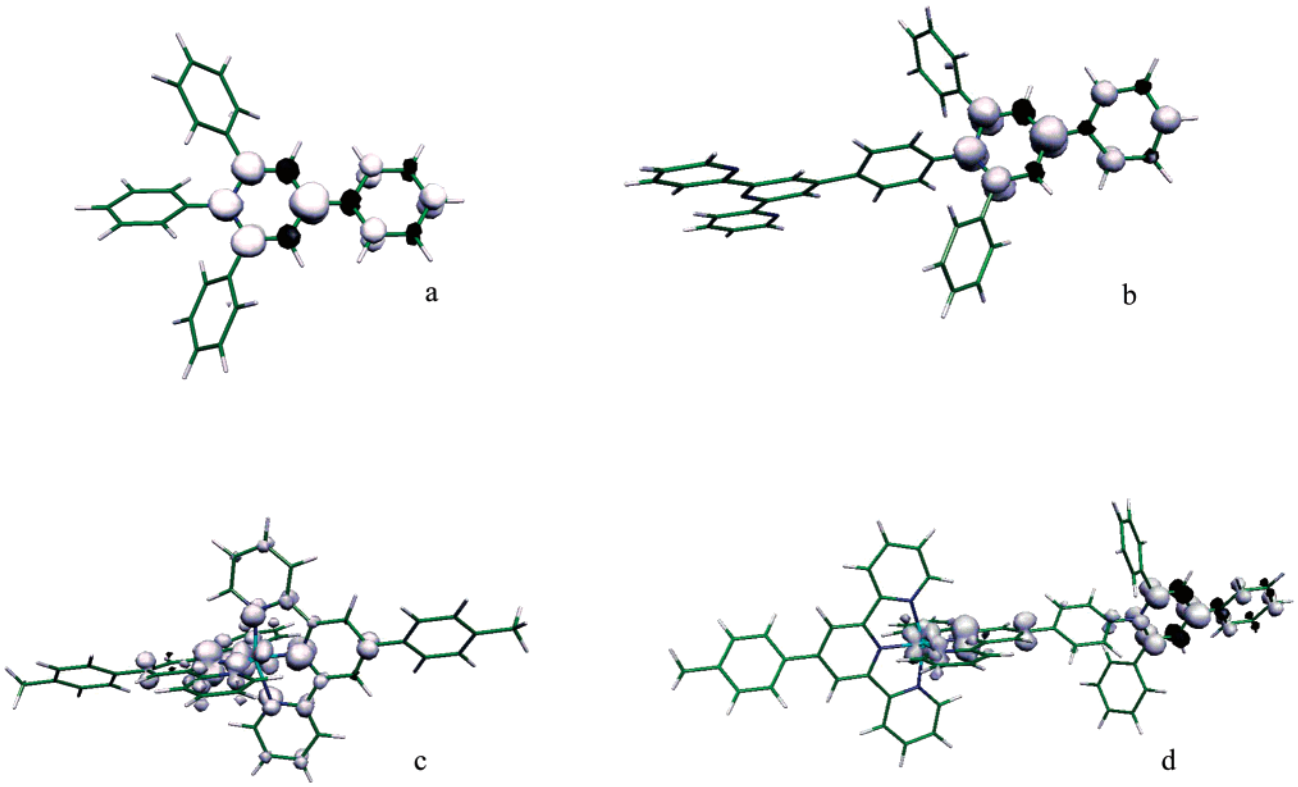

Figure 2. Computed spin density distribution for the reduced species: (a) [**A**]$^-$ model acceptor; (b) [**L1A**]$^-$ ligand; (c) [**P1/Os**]$^-$ reference photosensitizer; and (d) [**P1A/Os**]$^-$ dyad. Contour value: 0.005 au for [**A**]$^-$ and [**L1A**]$^-$; 0.0025 au for metal complexes.

linked to the H_3TP^+ moiety (θ_{0P1A}) than for the one of the Me-ptpy ligand (θ_{0P1}). On adding the torsion angles around the phenyl spacer linked to the acceptor, θ_{0P1A} ($\approx 36°$) and θ_1 ($\approx 67°$), the pyridinium ring was shown to be practically orthogonal to the tpy plane thus confirming the expected almost complete geometrical decoupling of the acceptor fragment from the photosensitizer subunit. It remains nonetheless that the calculated value for θ_1 is significantly underestimated (by ca. 20°) in comparison with both solid-state and solution experimental data.[25] This discrepancy could be an indication either of a floppy torsion, strongly affected by environmental effects (crystal packing or solvent),[68] or, more likely, of an overestimation of the conjugation effects.[72] However, the consequences of such a difference on the intercomponent electronic coupling are limited, since the $\pi-\pi$ interaction, by far the most important contribution to the electronic coupling between P1 and A, decays roughly as cos θ_1.[73]

Concerning the monoreduced acceptor dyad, [**P1A/Os**]$^-$, we did not expect significant structural relaxation upon reduction, as found above for the [**P1/M**]$^-$ systems. Nevertheless, it is a matter of fact that, upon reduction, a slight, but meaningful, flattening effect was computed for the reduced model acceptor (and ligand [**L1A**]$^-$). Thus, in the case of the dyad, a structural reorganization of the organic part of the ligand could not be ruled out, especially when the reduction process is expected to take place on the acceptor moiety.[26] This effect was also observed, on a short time scale, upon photoinduced transient reduction. For example, Vlcek,[74] McCusker,[75] and co-workers have evidenced subnanosecond intramolecular rotations coupled to PET or CT excitations within a Re(I) complex of related pyridinium-derivatized ligand and Ru(II) complex of 4,4′-diphenyl-2,2′-bipyridine, respectively. However, in the present case, the intramolecular rotation is largely hindered *in the ground state* (including the reduced form), and the computed effects of the structural relaxation upon the electronic properties for the reduced model acceptor were found to be very scarce as compared to that calculated with the X-ray structure of the native model acceptor. Therefore, the optimized structure of the nonreduced (i.e. native) system, **P1A/Os**, could reasonably be used to compute the UV−vis spectra of the reduced complex [**P1A/Os**]$^-$.

4.2. Electronic Features: Molecular Orbital Analysis and Spin Density Distribution. When analyzing the electronic structure of the **P1/M** molecules, we observed all systems exhibit the typical well-known features of a pseudo-octahedral d^6 metal complex of polypyridyl ligands: the HOMO is a metal centered d_π orbital and the LUMO is a π^* orbital centered on tpy ligands.

The situation becomes more interesting for the reduced systems. In particular, the reduction of both the isolated model acceptor (**A**) and the related A-functionalized ligand (**L1A**) leads to very similar distributions of spin density (see Figure 2, a and b), which are typically localized on the pyridinium ring and its attached terminal phenyl ring (at position 4). This localization correlates previous EPR measurements performed on a chemically reduced dye derivative of the model acceptor.[76]

(72) Geskin, V. M.; Bredas, J. L. *Int. J. Quantum Chem.* **2003**, *91*, 303−310.
(73) Woitellier, S.; Launay, J.-P.; Joachim, C. *Chem. Phys.* **1989**, *131*, 481−488.
(74) (a) Liard, D. J.; Busby, M.; Farrell, I. R.; Matousek, P.; Towrie, M.; Vlcek, A., Jr. *J. Phys. Chem. A* **2004**, *108*, 556−567. (b) Busby, M.; Liard, D. J.; Motevalli, M.; Toms, H.; Vlcek, A., Jr. *Inorg. Chim. Acta* **2004**, *357*, 167−176.
(75) Damrauer, N. H.; McCusker, J. K. *J. Phys. Chem. A* **1999**, *103*, 8440−8446.
(76) Bock, H.; Herrmann, H.-F. *Helv. Chim. Acta* **1989**, *72*, 1171−1185.

Moreover, the nonnegligible spin density contribution computed on the carbon atom in position 4 of the pyridinium ring is consistent with a resonance quinoidal form (see Scheme 1). These results also confirm that the geometrical decoupling of the acceptor is accompanied by a noticeable electronic decoupling, since no significant spin density was found on the tpy moiety when reducing the **L1A** ligand. In other words, the acceptor moiety retains its main electronic characteristics and it is decoupled from the rest of the ligand even though it is covalently linked to the tpy units. Subsequently, the same inclination is expected for the forthcoming corresponding complex photosensitizer, P1, although the complexation process is known to exert an electron-withdrawing influence upon the electronic properties of A. Experimentally, this effect was evidenced by performing electrochemical measurements.[26]

The calculated spin density for the reduced [**P1/Os**]$^-$ and [**P1A/Os**]$^-$ complexes is illustrated in Figure 2 (c and d). The reduced [**P1/Ru**]$^-$ species is not reported, since it is practically identical to [**P1/Os**]$^-$, the only appreciable difference being the spin density located on the metal atom: 0.02 au for [**P1/Os**]$^-$ versus 0.01 au for [**P1/Ru**]$^-$. This result is consistent with both the greater bonding and back-bonding interactions of Os as compared to Ru and the smaller M−N bond length values found for the Os-based complexes (see for instance ref 48). When observing Figure 2c, it can be noted that the spin density computed for [**P1/Os**]$^-$ is mostly localized on the tpy rings, in accordance with the tpy-π^* nature of the LUMO of the nonreduced (i.e., native) species.

On replacing ligand **L1** by **L1A**, the distribution of spin density of the reduced [**P1A/Os**]$^-$ is expected to sharply differ from that of [**P1/Os**]$^-$, as the first reduction process is no longer assumed to occur on the P1/Os photosensitizer but on the acceptor group. Indeed, spin density was found to be almost completely localized on the ligand bearing the acceptor moiety (**L1A**) with 14% on the pyridinium itself and 70% on the tpy moiety (see Figure 2d). A small but nonnegligible spin density was also encountered on the phenyl (spacer) that connects the H_3TP^+ moiety to the tpy. More surprisingly, 12% of the spin density was also computed on the metal center. All these evidences are consistent with a description of the reduction of **P1A/Os** as *mainly* consisting in a reduction of the acceptor moiety.[77] Brought together, these issues are in accordance with the experimental outcomes,[26] as it was shown that, upon monoelectronic reduction, the resulting [**P1A/Os**]$^-$ species was displaying the spectroscopic signatures of both the reduced acceptor and also, unexpectedly, that of the reduced chromophore [**P1/Os**]$^-$ (see below, section 4.5).

A striking point, however, is the fact that different patterns for the spin density are computed for the reduced photosensitizer unit, P1, depending on whether this latter is isolated or embedded within the dyad system. Indeed, the spin density located on the Os center within [**P1A/Os**]$^-$ was found to be considerably larger (0.12 au) than that computed for the reduced parent [**P1/Os**]$^-$ (0.02 au). Thus, paradoxically, the calculated Mulliken charge of the metal ion is smaller within the reduced acceptor dyad than it is within [**P1/Os**]$^-$. Together with the previously noticed propensity computed for the reduced model acceptor to adopt a flattened geometry and alternate short/long bond length pattern, the latter spin density map could be consistent with a quinoidal-like contribution[69,78] (see Scheme 1) in which the electron injected onto the acceptor (electrochemically or photochemically) is formally (back)transferred to the metal ion. The fact that such a peculiar spin distribution was identified for the dyad under its native geometry (no structural optimization was performed for the reduced form) is not surprising, since the structural relaxation is a consequence of electronic redistribution,[79] usually resulting from a reductive primary electron transfer, as exemplified by the behavior of the *N*-methyl-4,4′-bipyridinium ligand (MQ^+) within [Re(MQ^+)-$(CO)_3$(dmb)]$^{2+}$.[74]

Therefore, even if the acceptor moiety is retaining almost entirely its properties within the **P1A/Os** native system, part of the spin density is back-transferred from the reduced acceptor to the metal center through the phenyl spacer in the case of the [**P1A/Os**]$^-$ form. This points out the difficulty of defining the role of the phenyl group in the whole process, as already discussed from an experimental point of view. Indeed, in agreement with the experimental findings, our results show that the phenyl not only is a *simple spacer* within the supramolecular system but also takes an active part, as a full bridging component, in the electronic communication. Concomitantly, it also behaves as a full part of both the acceptor (electronic substituent effect)[26] and the photosensitizer (antenna effect).[11c,25,26,70] The fact that the insulating properties of the spacer are apparently of fluctuating efficiency depending on the reduction state of the acceptor is likely to have some consequences upon the photophysical properties of the dyad. More specifically, this changing behavior may partly explain the experimentally inferred fast rate for the backward electron-transfer process to the ground state (i.e., the charge recombination process, *[$P1^+-A^-$] → [P1−A]) following the postulated CS step ([P1−A] → *[$P1^+-A^-$]).[26] It is therefore of interest to investigate the similarities between the singly occupied molecular orbital (SOMO) of the reduced species and the LUMO of the corresponding native parent species in order to establish whether the picture drawn out of the (spectro)-electrochemical experiment can be extrapolated to the photoinduced processes.

4.3. Spectral Signatures of Acceptor-Based Organic Molecules. The computed UV−vis spectra of the model acceptor $[H_3TP\text{-}p]^n$ and the acceptor-substituted ligand $[H_3TP\text{-}ptpy]^n$, in both their native ($n = +1$) and reduced ($n = 0$) forms, are plotted in Figure 3a and reported in Table 2. Experimental absorption spectra of $[H_3TP\text{-}p]^+$ and $[H_3TP\text{-}p]^0$ are shown in Figure 3b. The spectra of the reference species (**A**) and related ligand (**L1A**) look very similar. In fact, both $[H_3TP\text{-}p]^+$ and $[H_3TP\text{-}ptpy]^+$ show a set of closely lying intense electronic transitions in the region between 330 and 300 nm, the most intense ones being at 325 and 320 nm, respectively. The overall shape of the resulting simulated spectra (with fwhm = 0.15 eV) for $[H_3TP\text{-}p]^+$ and $[H_3TP\text{-}ptpy]^+$ display a single absorption band with a maximum at 325 and 315 nm, respectively. These computed spectra match well the corresponding experimental

(77) It is worth noting that the computed pattern of the spin density for the reduced species slightly differs from that of the SOMO, as expected, due to spin polarization effects. In particular, there is a larger contribution of both the tpy ligand and metal ion to the SOMO than to the total spin density. It remains nonetheless that the SOMO computed in the case of the reduced **P1A/Os** species includes a significant contribution of the pyridinium ring.

(78) Ward, M. D. *Chem. Soc. Rev.* **1995**, 121−134.
(79) Vlcek, A., Jr. *Coord. Chem. Rev.* **2000**, *200−202*, 933−977.

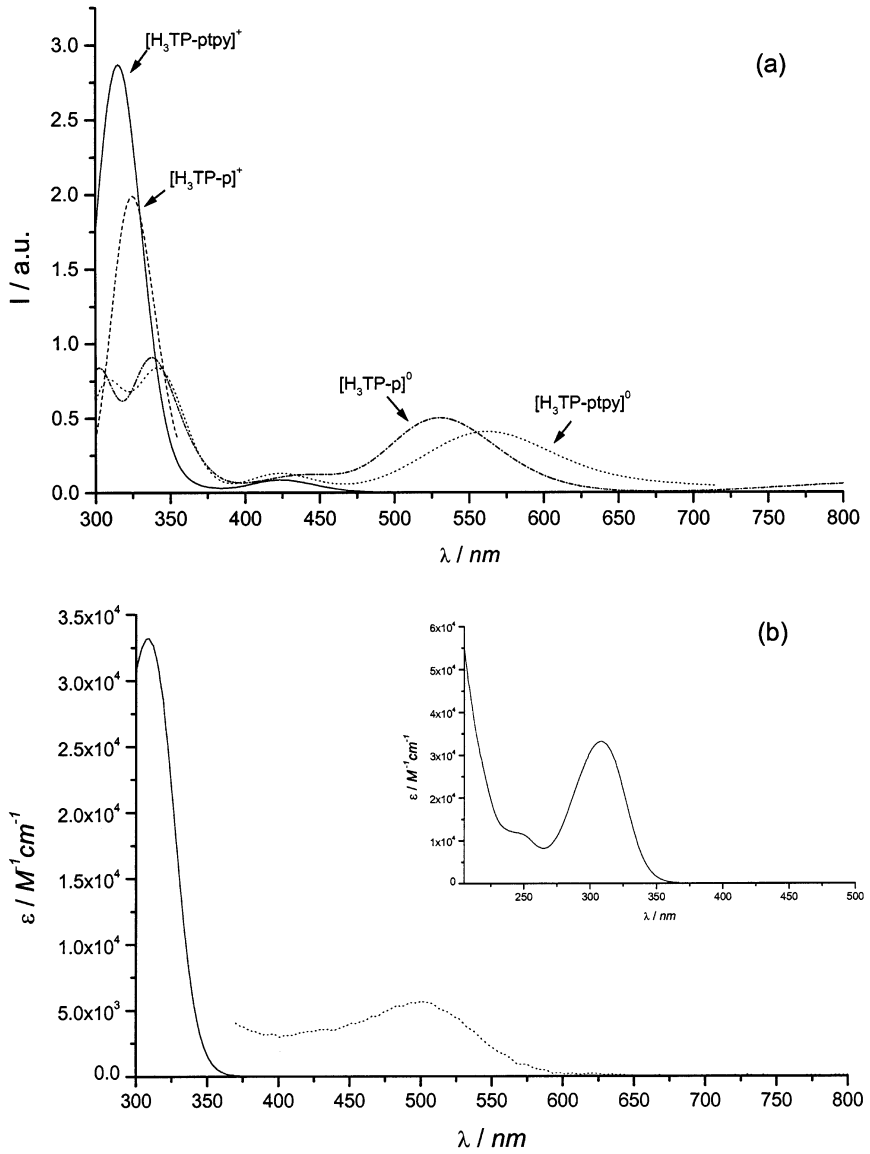

Figure 3. (a) Computed UV−vis absorption spectra (fwhm = 0.15 eV) of $[H_3TP\text{-}p]^n$ and $[H_3TP\text{-}ptpy]^n$ both in their native ($n = +1$) and monoreduced ($n = 0$) forms. (b) Experimental absorption spectra of $[H_3TP\text{-}p]^+$ (CH_3CN solution) and $[H_3TP\text{-}p]^0$ (reduced at $E = -1.0$ V vs SCE in CH_3CN + 0.1 M $TBABF_4$).[26] Inset: overall absorption spectrum of $[H_3TP\text{-}p]^+$ (CH_3CN solution).

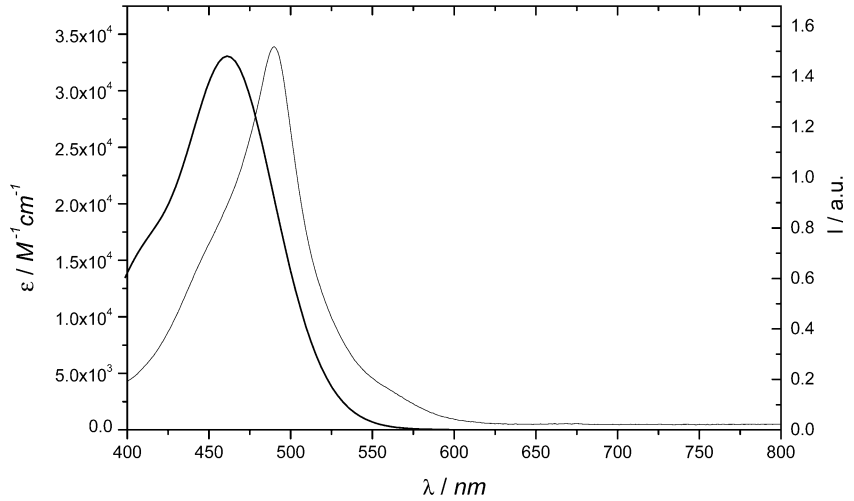

Figure 4. Absorption spectra of **P1/Ru** native complex. (Simulated) with fwhm = 0.15 eV (bold solid line). (Experimental) acetonitrile solution (solid line).

ones that also show single absorption bands at 308 nm ($R = -5.2\%$) and 309 nm ($R = -1.9\%$), respectively.

All these *intense* transitions correspond to excitations involving orbitals centered on the acceptor moiety only. Regarding

Table 2. Principal Computed Electronic Transitions (in nm) and Associated Oscillator Strength (*f*) in Parenthesis, along with Absorption Maxima for Simulated (λ_{sim}) and Experimental (λ_{exptl}) Absorption Bands of **A**, **L1A**, $[\mathbf{A}]^-$, and $[\mathbf{L1A}]^-$ Together with Corresponding Reliability Factors, *R* (in %)

entry	λ (*f*)	λ_{sim}[a]	λ_{exptl}[b]	*R*
A	325 (0.36)	325	308	−5.2
	318 (0.26)			
$[\mathbf{A}]^-$	526 (0.15)	528	503	−4.7
	455 (0.007)/444 (0.03)	448w	no	
	326 (0.31)	338	nd	
	302 (0.23)	302	nd	
L1A	423 (0.03)	423w	no	
	320 (0.31)	315	309	−1.9
	314 (0.30)			
	304 (0.20)			
$[\mathbf{L1A}]^-$	568 (0.10)/551 (0.03)	563/548sh		
	424 (0.05)	424w		
	350 (0.15)	341		
	336 (0.16)			
	307 (0.20)	310		

[a] fwhm = 0.15 eV. [b] References 25 and 26. w: weak. no: not observed. nd: not determined (see text). sh: shoulder.

Table 3. Principal Computed Electronic Transitions (λ, in nm) and Associated Oscillator Strength (*f*) along with Absorption Maxima (in nm) for Simulated (λ_{sim}) and Experimental (λ_{exptl}) Absorption Bands and Corresponding *R* Factors (in %) for the Native Forms of the **P1/M** and **P1A/Os** Complexes

entry	λ	*f*	λ_{sim} (fwhm in eV)	λ_{exptl}[a]	*R*
		$S_0 \rightarrow S_n$ transitions			
P1/Ru	464	0.49	461 (0.15)	490	6.3
	408	0.22			
P1/Os	501	0.34	471 (0.20)	490	4.0
	444	0.34			
P1A/Os	500	0.34	468 (0.20)	492	5.1
	435	0.38			
	353	0.28	349 (0.20)	314	−10.3
	347	0.60			
		$S_0 \rightarrow T_1$ transitions			
P1/Os	710 (615)[b]			668	−5.9[c] (+8.6)[b,c]
				645	
P1A/Os	736 (650)[b]			668	−9.2[c] (+2.8)[b,c]
				645	

[a] Experimental values are taken from refs 25 and 26. [b] ΔSCF values. [c] Calculated with computed *transition* energies, with respect to the energy of the main ^{3}MLCT experimental *band* (at 668 nm).

L1A, tpy-centered transitions are of lower intensity than A-centered ones and appear at higher energy in the 313−219 nm range. Noteworthy, the most intense transitions are related to one-electron excitations from doubly occupied MOs to the LUMO, this latter being located on the pyridinium ring and its terminal phenyl substituent (at position 4), which are conjugated together ($\theta_4 \approx 29°$). The fact that the MOs of the chelating tpy fragment do not play a major role in these processes may be viewed as further evidence of the rather pronounced electronic decoupling of the acceptor moiety from the rest of the ligand.

As is the case for the native $[H_3TP\text{-}p]^+$ and $[H_3TP\text{-}ptpy]^+$ species, the computed reduced forms also show absorption in the UV region between 300 and 350 nm. Two transitions of comparable intensity, giving rise to two bands instead of a single one, are calculated at 302 and 326 nm for $[H_3TP\text{-}p]^0$ and at 307 and 336 nm for $[H_3TP\text{-}ptpy]^0$. All these transitions correspond to excitations from doubly occupied orbitals to the SOMO. The spectra of $[H_3TP\text{-}p]^0$ and $[H_3TP\text{-}ptpy]^0$ are also expected to display a broad band resulting from several transitions situated between 500 and 600 nm. In the case of $[H_3TP\text{-}p]^0$, the most intense computed transition is at 526 nm ($f = 0.15$) very close to the maximum in the simulated spectrum obtained by using a fwhm of 0.15 eV (528 nm). Regarding $[H_3TP\text{-}ptpy]^0$, the most intense computed transition is at 568 nm ($f = 0.10$), while the maximum in the simulated spectrum is at 563 nm (with fwhm = 0.15 eV). In both systems, the most intense transition is related to the excitation of the unpaired electron from the pyridinium-centered SOMO to a higher, unoccupied MO located on the acceptor moiety. As expected, the SOMO of $[H_3TP\text{-}p]^0$ closely resembles the LUMO of $[H_3TP\text{-}p]^+$. In other words, one is allowed to believe that the previously[26] observed spectral features obtained out of electrochemical reduction accurately reproduce the effects of a reduction originating from an intramolecular photoinduced electron transfer from *P1. Indeed, experimentally, $[H_3TP\text{-}p]^0$ (Figure 3b) does exhibit the supplementary broad adsorption band expected in the visible region, which was observed at 503 nm.[26] This value fits well to the computed one ($R = -4.7\%$).

In short, the main computed effect of the reduction process on the UV−vis spectra of model acceptor (**A**) and related ligand (**L1A**) stems from the rise of a new broad band at ca. 500 nm ascribed to pyridinium-centered electronic transitions from the SOMO to virtual MOs.

4.4. Spectral Signatures of the Native Ru(II) and Os(II) Complexes. The calculated energies and oscillator strengths (*f*) of the principal electronic transitions together with the corresponding experimental values[25] for **P1/M** (M = Ru, Os) and **P1A/Os** are reported in Table 3.

Concerning the most intense transitions for both Os and Ru compounds (at ca. 460 and 500 nm; see Table 3), a good agreement between the computed and the experimental data can be found, the largest difference being ca. 30 nm ($R = +6.3\%$). Moreover, the shapes of simulated bands also closely reproduce the experimental profiles (see Figure 4).

For all systems, transitions calculated in the spectral region ranging from 400 to 500 nm are of MLCT character. They are ascribed to one-electron excitations from doubly occupied mainly metal-centered orbitals (65% − 85%) to empty π^* orbitals of the tpy. The first main transition (at lower energy) has a dominant contribution of the HOMO−LUMO type. In the case of symmetric compounds (**P1/M**), the empty π^* orbital has contribution from both tpy systems, similarly to other symmetric Ru complexes such as $[Ru(bpy)_3]^{2+}$.[45a] In the case of **P1A/Os**, the symmetry breakdown due to the presence of the acceptor group on one of the two tpy ligands causes a localization of the LUMO. Indeed, the largest contributions of ligand-centered molecular orbitals to the MLCT bands are found to mainly originate from H_3TP^+-ptpy. Thus, the first intense transition at 500 nm ($f = 0.34$) is mainly centered on the tpy fragment of the H_3TP^+-derivatized ligand. More interestingly, transitions corresponding to the *direct electron transfer from the metal center to the acceptor moiety (A*) are also computed to occur at higher energy (at 353 nm), but with a smaller intensity ($f = 0.28$). They could not be detected in the experimental spectrum due to the closely lying much stronger transition computed at 347 nm ($f = 0.6$) and other LC transitions (not computed for the dyad; see Table 2). A plot of the orbitals involved in these two intense transitions is given in Figure 5.

It is worthwhile to note that, for all systems, the band located around 490 nm is resulting from the superposition of several

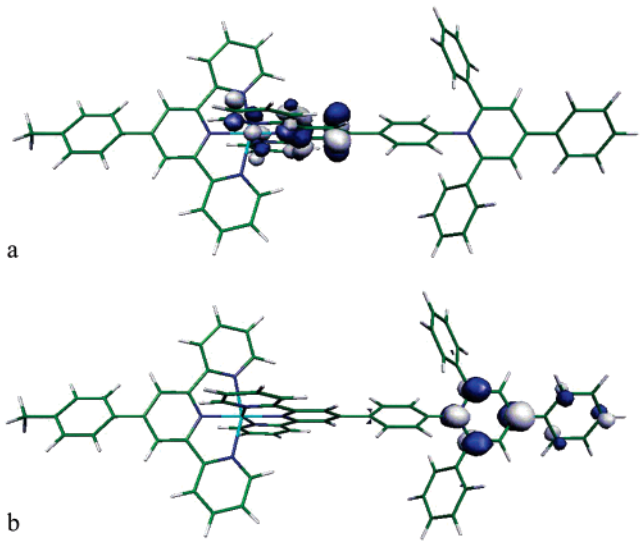

Figure 5. Virtual orbitals predominantly involved in the MLCT transitions of **P1A/Os** computed at 500 nm (a) and 353 nm (b). Isosurface contour value of 0.05 au.

rather intense transitions (*f* ranging from 0.2 to 0.5) whose spacing increases in going from **P1/Ru** to **P1/Os** and to **P1A/Os**. When the oscillator strengths of the two transitions are of comparable magnitudes (as for **P1/Os** and **P1A/Os**), the band is expected to display a symmetric shape. For **P1/Ru**, where the two transitions have very different oscillator strengths, an asymmetric band shape is foreseen, which is indeed found to be in agreement with the experimental data (see Figure 4).

Singlet-to-triplet transitions have been computed only for **P1/Os** and **P1A/Os** and compared to the available experimental data. These bands are not experimentally detected for Ru(II) bis-terpyridyl chromophores, due to the small spin−orbit coupling of Ru. As the spin−orbit coupling is not explicitly taken into account in our calculations, all singlet-to-triplet transitions are computed to be forbidden with zero associated oscillator strength. A ΔSCF procedure, that is, the calculation of the singlet−triplet transition as the difference in energy of the triplet and singlet states, was also applied in order to compute the first transition energy (Table 3). It was found that the transition energies are systematically underestimated when using the TD-DFT approach (up to 68 nm i.e., 0.17 eV), whereas the ΔSCF procedure provides overestimated energies of transitions (up to 53 nm, i.e., 0.16 eV).

4.5. Spectral Signatures of the Monoreduced Ru and Os Complexes. Experimentally, the spectroelectrochemical study of the various compounds was undertaken in order to record their electronic spectra when reduced at such a controlled potential that only the corresponding monoreduced species were expected to be generated. From both computational and experimental results, it appears that, upon reduction, the spectroscopic properties of the chromophores are strongly modified. Namely, besides the overall decrease in the intensity of the various transitions, which was already noticed for the reduced model acceptor, the theoretical calculations are also anticipating the rising of a broad new band in the NIR region. These main features are found to be in good agreement with the experimental data.[26,80]

More precisely, in the case of the [**P1/Ru**]$^-$ and [**P1/Os**]$^-$ reduced model photosensitizers, new transitions are computed between 600 and 800 nm. The most intense simulated band (fwhm = 0.1 eV) in this range is predicted at 671 nm for [**P1/Ru**]$^-$ and 634 nm for [**P1/Os**]$^-$ and is ascribed to a SOMO to π^*, ligand centered transition. Noteworthy, time-resolved transient absorption difference spectra recorded for the photoexcited *[**P1/M**] systems[26,70,81] exhibit a positive feature at around 600 nm, which is usually ascribed to the spectroscopic signature of the reduced ligand [**L1**]$^-$. This assignment was made by analogy to the spectral absorption of both the chemically produced radical anion of the para-substituted ptpy ligand[82] [R-ptpy]$^-$ and the features of [bpy]$^-$ within photoexcited *$[Ru(bpy)_3]^{2+}$.[3a] Therefore, as was found in the case of the model acceptor (section 4.3), SOMO-to-π^* electronic transitions within *reduced* complexes (i.e., related to spectral features obtained out of electrochemical reduction) correctly reproduce transient spectral characteristics of a metal-to-ligand charge-transfer state (involving the ligand-centered LUMO) of the photoexcited *native form* of complex photosensitizers.

However, it is worth keeping in mind the following facts about [**P1/Os**]$^-$. First, Os(II)-based complexes show, at least in their natives forms, some absorption in the NIR region originating from singlet to triplet MLCT transitions. Second, within the experimental conditions of the spectroelectrochemical study, both the reduced and native species are present and mixed together (i.e., the monoreduced species cannot be quantitatively obtained, i.e., in a pure form, for thermodynamic reasons, due to the close value of first and second reduction potentials).[26] By determining the relative abundance of these two species in the reaction medium, we could nevertheless *roughly* establish the main spectral features of the pure reduced species, [**P1/Os**]$^-$.[26] But, in the last analysis, the broad bands recorded in the 600 to 800 nm region could not be definitely attributed to the reduced species only. *Thus, in this case, only theory allows us to show how reduced species are expected to absorb in this region and suggests that the broad bands around 600−700 nm are their first characteristic signature.*

To further validate the theoretical hypothesis, the UV−vis spectroelectrochemical study of the **P1/Ru** chromophore has been performed. **P1/Ru** shows the advantage of having no absorption in the NIR, which could be related to the singlet-to-triplet transition. Any band arising in the 500−800 nm region during the reduction process can therefore straightforwardly be ascribed to the reduced form [**P1/Ru**]$^-$. A broad band (max 723 nm/760 nm) is indeed experimentally detected (Figure 6). Thus, *the cross experimental−theoretical comparison confirms the predictive quantitative and qualitative values of the computational procedure. It also further demonstrates that taking the Ru(II) compounds as analog species for modeling the related Os(II)-based complexes is a sound strategy.*

The other more intense bands, in the different spectra, are situated in the spectral region ranging from 400 to 500 nm. As previously discussed in the case of the native species, these bands, of MLCT character, are actually resulting from several transitions, two of them being predominant. Nevertheless, two

(80) Similar NIR absorption emerging upon reduction has been recently reported for iron(II) and cobalt(II) complexes with oligopyridyl-like ligands (see: Ruben, M.; Breuning, E.; Barboiu, M.; Gisselbrecht, J.-P.; Lehn, J.-M. *Chem.−Eur. J.* **2003**, *9*, 291−299).
(81) Collin, J.-P.; Guillerez, S.; Sauvage, J.-P.; Barigelletti, F.; De Cola, L.; Flamigni, L.; Balzani, V. *Inorg. Chem.* **1992**, *31*, 4112−4117.
(82) Amouyal, E.; Mouallem-Bahout, M.; Calzaferri, G. *J. Phys. Chem.* **1991**, *95*, 7641−7649.

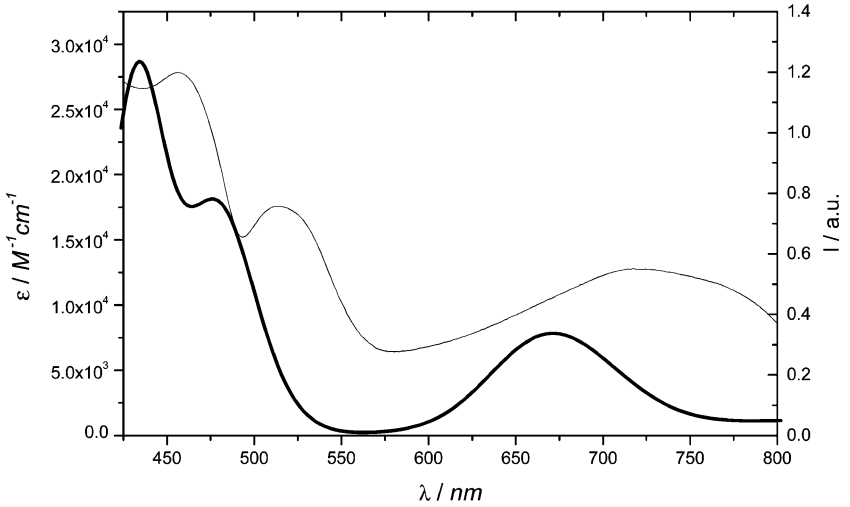

Figure 6. Absorption spectra of [**P1/Ru**]$^-$ reduced chromophore. Computed (bold solid). Spectroelectrochemistry (solid): $E = -1.2$ V vs SCE in CH_3CN + 0.1 M $TBABF_4$.

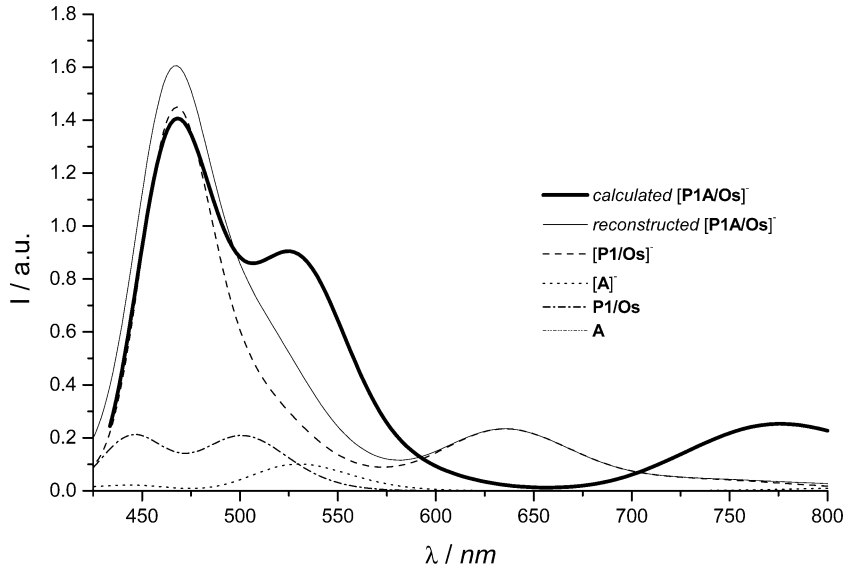

Figure 7. Simulated absorption spectra (fwhm = 0.1 eV) of reduced [**P1A/Os**]$^-$. Calculated (bold solid) and reconstructed (solid) from weighted contributions of parent chromophoric species (dotted).

main differences with respect to the native form must be pointed out. On one hand, both transitions are shifted toward lower energies when going from the native to the reduced species,[83] the one at higher energy being more shifted than the other. On the other hand, the relative intensities of the transitions are strongly modified. In the case of the ruthenium complexes, in going from the native to the reduced [**P1/Ru**]$^-$ species, the most intense transition, located at lower energy, decreases in intensity while the other increases. In fact, the MLCT band of asymmetric shape, computed at 461 nm with a shoulder toward higher energies in the former case, is blue-shifted by ca. 25 nm (about 0.17 eV) to 434 nm in the reduced species while showing a shoulder toward lower energies. *It is also noteworthy that these data are in agreement with the experimental spectra, for both band shapes and transition energy shifts.* In the case of [**P1/Os**]$^-$, similar but more pronounced trends are found. The two transitions of roughly the same intensity in the native species are changed into one strong transition at higher energy (467 nm, $f = 0.37$) and another one of very low intensity (515 nm, $f = 0.06$) for [**P1/Os**]$^-$. As a consequence, a red-shifted band (by ca. 25 nm) displaying an almost symmetric shape was found for the reduced species, in agreement with the experimental data.[26]

The computed spectrum of [**P1A/Os**]$^-$ is reported in Figure 7. For comparison purposes, the spectrum was also reconstructed starting from the weighted contributions of the reduced parent chromophores. It was built up from the different proportions deduced from the spin density map of [**P1A/Os**]$^-$ (see section 4.2.): 86% of [**P1/Os**]$^-$ and 14% of [**A**]$^-$ for the reduced forms, together with 14% of **P1/Os** and 86% of **A** (not absorbing in the visible range) for the complementary contribution of the native forms.

As it can be noted, the sum of the weighted contributions (reconstructed spectrum) does not match the simulated spectrum

(83) For these MLCT transitions, upon reduction, the computed (mainly) metal-centered HOMO is found to be more destabilized than involved ligand-centered higher lying π^* orbitals. This finding is reminiscent of previous experimental issues for a series of substituted Ru(II) bis-terpyridyl complexes (see: Maestri, M.; Armaroli, N.; Balzani, V.; Constable, E. C.; Cargill Thompson, A. M. W. *Inorg. Chem.* **1995**, *34*, 2759−2767). It means that, when reduced, the triphenylpyridinium radical anion ($[H_3TP]^0$) is apparently worth considering as an electron-donating group. Similar bathochromic shift of the MLCT band has been also reported in going from **P1/M** to affiliated donor dyads, **P1D/M**, with D = NMe_2 (see ref 25).

Table 4. Principal Computed Electronic Transitions (λ, in nm) and Associated Oscillator Strength (f) along with Absorption Maxima (in nm) for Simulated (λ_{sim}) and Experimental (λ_{exptl}) Absorption Bands and Corresponding R Factors (in %) for the Reduced Form of the **P1/M** and **P1A/Os** Complexes

entry	λ	f	λ_{sim}[a]	λ_{exptl}	R
[P1/Ru]$^-$	818/671	0.01/0.08	671	760/723[b]	13.3/7.8
	480	0.15	477	515[b]	8.0
	434	0.24	434	457[b]	5.3
[P1/Os]$^-$	960	0.03	nd	nd	nd
	740	0.01	740sh	760[c]	2.7
	635	0.06	634	600[c]	−5.4
	515	0.06	515	505[c]	−1.9
	467	0.37	469	455[c]	−3.0
[P1A/Os]$^-$	779	0.06	775	760[c]	−1.9
	539	0.07	525sh	id[c]	nd
	531	0.07			
	475	0.12	468		
	461	0.22			

[a] fwhm = 0.1 eV. [b] This work. [c] Reference 26. nd: not determined. sh: shoulder. id: ill-defined spectum.

computed for the reduced dyad. This indicates that **[P1A/Os]**$^-$ should no longer be considered as a supramolecular species[1,4,11] as was the case for its native form.[25,26] Upon reduction, the initially rather independent P1/Os and A components are coming on electronically and, noticeably, interact through the phenyl "spacer", as previously revealed (section 4.2; see also below). Such an inference could actually be experimentally substantiated from spectroelectrochemistry performed on the dyad and more precisely from the incongruent[84] presence of the reduced photosensitizer. Although partial delocalization of electrons added onto A over the P1 unit has been postulated,[26] its significance was, at that time, underestimated.

Within the 430 nm to 850 nm spectral range, two intense bands are predicted: an almost symmetrical one at ca. 775 nm and another one at 468 nm, roughly 3 times more intense, with a shoulder outlined at about 525 nm. These bands originate from the three sets of intense transitions reported in Table 4. The first absorption band around 775 nm is mainly resulting from an SOMO-to-π* transition computed at 779 nm, the involved π* molecular orbitals being mainly localized on the phenyl (spacer) of the H_3TP^+-ptpy ligand. As a matter of fact, the presence of A on the ptpy ligand strongly affects the energy of this first transition. The same SOMO-to-π* transition was actually also computed in absence of the acceptor, for **[P1/Os]**$^-$, but at significantly higher energy (634 nm). However, contrary to **[P1/Os]**$^-$ for which the two Me-ptpy ligands have a share to the π* orbital involved in the transition, in the case of the reduced dyad **[P1A/Os]**$^-$, the implicated π* MO is only localized on the phenyl of the ptpy bearing the acceptor. The second set of intense transitions makes up the shoulder (outlined at 525 nm) of the band situated at 468 nm. Although the concerned transitions are MLCT in nature (the most intense ones being computed at 539 and 531 nm), the metal-centered orbital has nevertheless a significant contribution from the phenyl spacer that connects the acceptor. From the sole experimental data, it would be tempting to ascribe this shoulder to acceptor-centered transitions, by analogy with the absorption spectrum recorded for the reduced model acceptor (Figure 3, Table 2). However, this attribution would not be consistent with the results of the present calculations. *Actually, the transitions from SOMO to the higher virtual MOs of the acceptor are found to occur at higher energy*, the most intense ones being typically located at 475 and 461 nm (third set of intense transitions). *The resulting band is simulated at 468 nm* (fwhm = 0.1 eV).

4.6. Insights into vis−NIR Spectroelectrochemical and Transient Absorption Features. Both the rather large contribution and the unusual profile determined for the absorption band initially ascribed[26] to *pure* $[A]^-$ within **[P1A/Os]**$^-$ and revealed by the visible−NIR spectroelectrochemical study of **P1A/Os** may be explained by the additional "tainting" contribution of above-identified transitions from SOMO to phenyl spacer centered π* orbitals. Indeed, the absorption spectrum of the reduced acceptor embedded within the reduced dyad was obtained by deducting the contributions of the various other identified parent chromophoric species, in that case not correctly considered as electronically independent entities.[26]

Similarly, in the light of gained new insights, together with the characteristic spectral features experimentally well established for both the reduced ligand $[ptpy]^-$ (also theoretically confirmed in this work, section 4.5) and the oxidized metal center[81] (not computed here), transient difference absorption spectra recorded for **P1A/Os**[26] can therefore be qualitatively reanalyzed as follows (Figure 8).

The absorption (*2R*) of the chromophoric reduced acceptor, $[A]^-$ (SOMO-to-π*(A) transitions) embedded within the dyad is computed to be *accidentally situated in the same region* as the ^{1}MLCT transitions (*2B*) of the native dyad **P1A/Os**, at about 468 nm (Tables 3 and 4), in accordance with experimental inference.[26] *Ceteris paribus*, it is then not surprising that the photoinduced formation of $[A]^-$, if it occurs, cannot be easily observed except via an apparent abnormally pronounced attenuation (instead of the usual effect)[11c] of the overall bleaching of the more intense ^{1}MLCT band (*2B*), as compared to the corresponding *2B* feature of reference isolated ***P1/Os**. The uneven profile of the latter bleaching feature, with an outlined shoulder at ca. 503 nm, is found to be consistent with the bleaching of a rather intense new ^{1}MLCT band computed at ca. 525 nm ($R = -4.2\%$), *3B*, specifically involving the phenyl *spacer*. This band (*3B*) is not present in the parent photosensitizer **P1/Os** and is maybe also partly responsible for the attenuated absorption feature observed for the band *3R*, which is ascribed to the spectroscopic signature of the reduced ptpy ligand. This noticeable weakening of feature *3R* is also consistent with the possible capture of the photoexcited electron by the acceptor. Bleaching features recorded around 670 nm (*4B*) correspond to the disappearance of the ^{3}MLCT band. In the near UV region, another particular feature can be noted when comparing the behavior of **P1/Os** to that of **P1A/Os**. A significant depletion at ca. 390 nm is observed for the dyad, which is formed within the time of the laser excitation (pulse duration of ca. 10 ns; $\lambda_{exc} = 308$ nm),[26] in the region where positive features normally dominate (*1R*). Indeed, this excited-state absorption, *1R*, corresponds to the well-established rising of the LM(Os^{3+})CT band[81] (correlated with the disappearance of the main ^{1}MLCT band, *2B*) together with some absorption (associated with features *3R* and *4R*)[70,81] characteristic of the formation of the radical anion of the phenyl-substituted tpy ligand ($[\mathbf{L1}]^-$).[11c,26] In the present case, the additional bleaching

(84) Electrochemical reduction of **P1A/Os** has been carried out at such a potential ($E = -1$ V vs SCE) that the P1 subunit was not expected to be concerned ($E_{1/2}(P1/Os^{0/-}) = -1.21$ V) but only redox processes attached to the TPH_3^+ group ($E_{1/2}(TPH_3^{+/0}) = -0.91$ V and $E_{1/2}(TPH_3^{0/-}) = -1.00$ V).

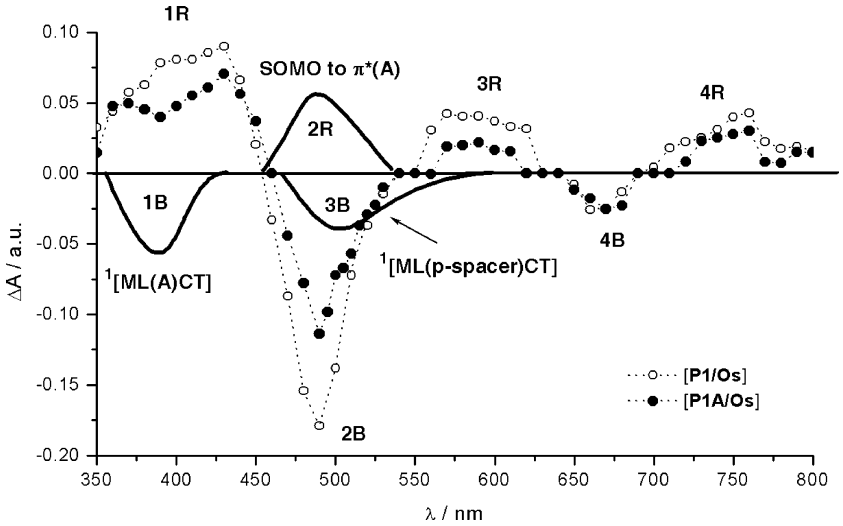

Figure 8. Schematic illustration of various identified contributions to transient absorption difference spectra of **P1A/Os** and reference **P1/Os** recorded at 20 ns after laser excitation (λ_{exc} = 308 nm) for isoabsorptive acetonitrile solutions.[26] Dotted lines: experimental features. Bold solid lines: new computed features specific to the dyad. For clarity, the computed bands schematically represented were subject to slight offsets along the λ axis to match experimental spectra.

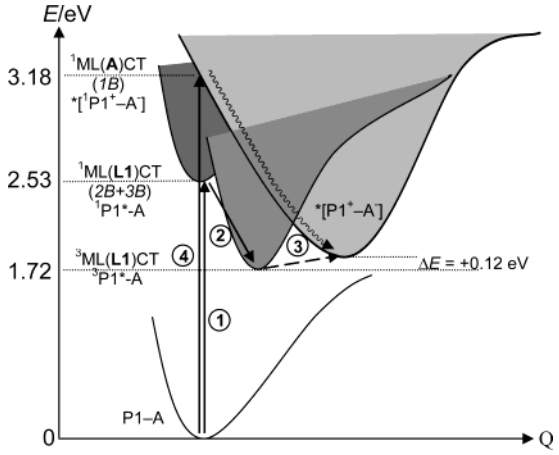

Figure 9. Potential energy curves representation of the two ET pathways proposed for CS formation within *[**P1A/Os**]: photoinduced (stepwise: 1 + 2 (intersystem crossing) + 3) and optical (direct: 4) processes. The given energy for the ^{3}ML(L1)CT state actually corresponds to the minimum $E_{em}(0-0)$ as experimentally determined in ref 26 (λ_{max} of emission at 77 K in BuCN frozen matrix). The energy difference, ΔE, between $E_{em}(0-0)$ and the CS state was determined in ref 26.

of the new band (*1B*) computed at 353 nm (see section 4.4; Table 3) and resulting from a direct optical charge transfer from Os(II) to the acceptor moiety of **L1A** well accounts for the depletion of *1R* features observed for **P1A/Os**, with an *R* factor of +10.5%.

The overall picture drawn out of the time-resolved transient absorption spectroscopy is compatible with the formation of the reduced acceptor although not straightforwardly observable[26] *due to unfavorable spectroscopic features. These findings are therefore consistent with the transient formation of the targeted charge-separated state, *[P1/Os$^+$–A$^-$].* To reach this hypothetical CS state, an alternative pathway to the classical stepwise photoinduced ET, involving the triplet MLCT state of *P1, is proposed: *the direct optical electron transfer from the ground state to the CS state (see Figure 9).* This theoretical issue is found to be consistent with available experimental data. Nonetheless, although slightly endoergonic by ca. 0.12 eV,[26] the photoinduced pathway seems to remain operative, as suggested, for instance, by the above-noticed sizable consumption of the photopromoted electron onto L1.[85]

5. General Comments

Besides the accurate reproduction of the experimental data, our theoretical results provide some information on the nature of the ground and excited states involved in photochemical processes taking place within reference photosensitizers, **P1/Os**, and acceptor dyad **P1A/Os**. Also, theoretical issues well reveal the actual nature of the electronic and geometrical coupling of the acceptor moiety with the photosensitizer. In particular, consequences of partial or residual conjugation are found to significantly affect the electronic properties of the molecules in their entirety, especially when single-electron reduced.

Structural optimizations performed on reduced species can be directly related to the relaxed *ground-state* geometries adopted by molecules on occasion of *steady-state* experiments, such as (spectro)electrochemistry. In the case of Ru(II) and Os(II) bis-terpyridyl complexes, **P1/M**, their structures were found to be almost unaffected by the monoelectronic reduction. Spectral features calculated for **P1/M** systems in their native and reduced forms well correlate with experimentally established electronic absorption spectra. For instance, the spectral signature usually ascribed, in time-resolved difference absorption spectra, to the reduced 4′-phenyl-tpy ligand (i.e., [L1]$^-$ radical anion) transiently generated by an intramolecular PET process is herein theoretically ground. This broad band situated around 600−700 nm is confirmed as being related to reduced ligand-centered SOMO-to-virtual higher lying π* orbital transitions.

More delicate is the case of acceptor dyads, **P1A/M**, where the pyridinium-based organic part is anticipated to be subject to some relaxation toward slightly flattened geometry upon reduction, as was theoretically postulated for the reduced model acceptor and related **L1A** ligand. Although the relative rates

(85) In ref 26, it is noteworthy that the substantial decrease of the emission quantum yield of *P1/Os within *[P1/Os-A] was measured for λ_{exc} = 600 nm, i.e., at lower energy than the ^{1}ML(A)CT electronic transitions. Therefore, the direct optical ET cannot account for such a decrease contrary to a possible PET process from *P1/Os to the covalently linked A unit.

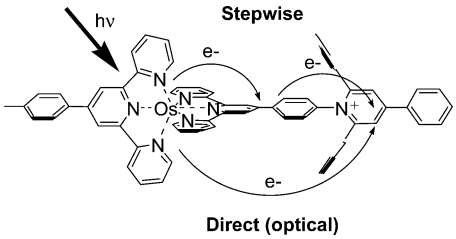

Figure 10. Schematic representation of stepwise and direct ET processes.

for intramolecular electronic redistribution and structural changes are not precisely known in the present case, the former is habitually assumed to propagate more rapidly than the latter, a fortiori when large molecular fragments such as the phenyl rings of the acceptor moiety are involved.[53,79] Thus, to figure out the *minimal* consequences of single-electron reduction upon the critical computed electronic properties of the acceptor dyad, the molecular geometry was not relaxed but frozen in the *optimized ground-state* conformation of the *native* form. Subsequent structural relaxation is merely amplifying electronic aftereffects.

Both computed spin density map and calculated electronic transitions clearly indicate that the added supplementary electron is almost completely delocalized over the whole [**P1A/Os**]$^-$ molecule. Therefore this system can no longer be considered as a true two-component system (i.e., dyad). There is actually a sizable interplay of the constituents through the phenyl spacer, which no longer fully plays the role of an insulating element. The valuable contribution of the theoretical analysis is here saliently illustrated by substantiating experimental findings hitherto not straightforwardly understandable.[26] From the detailed analysis of computed features of [**P1/Os**]$^-$ and [**P1A/Os**]$^-$ at both the structural (section 4.1) and electronic (section 4.2) levels, a formal mechanism for electronic delocalization could even be postulated. Namely, the rising out of partial quinoid (vs benzoid) contribution spreading from the experimental thermodynamic entry, [A]$^-$, over the metal center (Os^{2+}) of P1, is proposed. This point is of particular importance, since such an effect could explain the fast back electron transfer (CR step) inferred from photophysical investigations.[26,86]

When reduced, the **P1A/Os** system appears to behave as a made-in-one-piece electron-rich and polarizable molecule rather than a bipartite entity capable of undergoing a fully developed charge separation. This behavior is ascribed to combination of the intrinsically weak electron-withdrawing properties of A[26,84] with the possibly enhanced conjugation between P1 and A sequential to single-electron reduction. This latter effect remains possible despite the noticeable intramolecular steric hindrance however operative for the ground-state native form of the dyad. The heightened coupling through the -partially reduced- phenyl spacer is likely to favor the backward electron transfer (CR). It is also worth reminding that, in reality, the electron forwardly light-promoted onto A actually originates from the metal center of P1 and then oxidized into the attractive [P1]$^+$. The CR process is thus favored accordingly as compared to the electrochemically produced situation where the electron is provided by an external source (P1 is left unchanged before intramolecular electronic reorganization occurs).

It is worth stressing that the above-described behavior is concerned with the consequences of reduction of A within **P1A/Os**, thus mimicking the effects of the intramolecular-photoinduced and/or direct optical-ET process(es)[53] (see Figure 10) leading to the expected CS state previously postulated[26] and further substantiated in this work (section 4.6). The present analysis actually gives some new insights on the reasons why the photoproduced CS state is short-lived and eventually very rapidly formed (a direct optical ET may occurs; Figure 9). At the same time, a mechanism for efficient charge recombination (the contribution of a quinoid-like electronic redistribution; Figure 11) is proposed.

6. Conclusions

The most important outcomes of our work can be summarized as follows:

(i) role of the phenyl spacer in providing intercomponent coupling in the parent and reduced (and, presumably, excited) species;

(ii) direct optical excitation into the charge-separated state;

(iii) increase of the intercomponent coupling and electronic delocalization upon reduction;

(iv) involvement of the phenyl-spacer-to-π^* excitations in the spectral transitions of reduced and excited species;

(v) reinterpretation of the transient spectrum demonstrating the formation of the CS state;

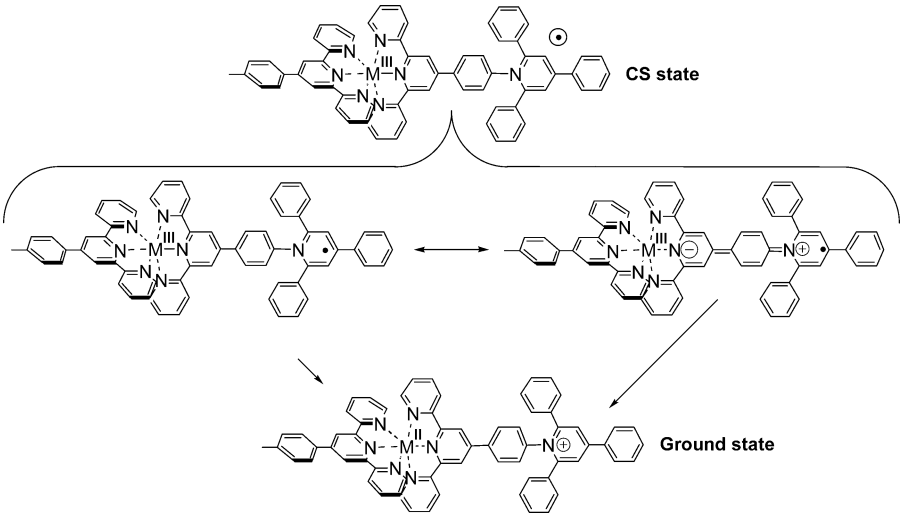

Figure 11. Schematic representation of backward ET processes from the CS state to GS (charge recombination) within *[**P1A/Os**]: proposed mechanism.

(vi) correlation between the *electronic* and *geometrical* decouplings.

This overall picture drawn out from the present theoretical study prepares general guidelines for forthcoming supramolecular engineering of the promising potentialities of triarylpyridinio-derivatized polypyridyl complexes of Ru(II) and Os(II). Dependent on whether targeted applications are directed toward nonlinear optics[27] or are aimed at achieving photochemical conversion of light energy, the properties of the supramolecular architecture will be tuned toward the search of *polarization effects* rather than obtaining *redox separated states*, respectively.

In consequence, to generate long-lived charge-separated states and overcome the above-reported dramatic drawbacks caused by residual intercomponent conjugation, the synthetic strategy currently developed consists of, concomitantly, the following:

(i) further increasing the steric hindrance around the intercomponent linkage to warrant as much as possible a strict orthogonality (geometrical decoupling and minimal overlap of π orbitals);

(ii) further strengthening the electron-withdrawing acceptors by varying peripheral substituents (R^1, R^2; Figure 1) borne by aryl fragments of the pyridinium moiety; this will also contribute to improving the pivotal spectroscopic signature of $[A]^-$, then easier to detect;

(iii) designing expanded redox cascades capable of delaying the undesired backward ET (i.e., the CR step) by undergoing long-range electron hopping, i.e., charge separation over longer distances.

(86) Work in progress.

Acknowledgment. The authors thank Prof. S. Campagna and Dr. F. Loiseau for stimulating discussions and the referees for useful comments. C.A. and I.C. are grateful to CNRS for financial support in the framework of the ACI "Jeune Équipe 2002" project and to the French National Computer Center (IDRIS) for a generous grant of computer time (project 41703).

Supporting Information Available: Computed bond length pattern for $[A]^-$ and $[L1A]^-$ reduced species. This material is available free of charge via the Internet at http://pubs.acs.org.

JA0482278